Rayleigh-Bénard convection and turbulence in liquid helium

R. P. Behringer

Department of Physics, Duke University, Durham, North Carolina 27706

Recent advances in the understanding of Rayleigh-Bénard convection and turbulence are reviewed in light of work using liquid helium. The discussion includes both experiments which have probed the steady flows preceding time dependence and experiments which have been directed toward understanding the ways in which turbulence evolves. Comparison is made where appropriate to the many important contributions which have been obtained using room-temperature fluids, and a discussion is given explaining the advantages of cryogenic techniques. Brief reviews are given for recent experimental investigations of convection in ^{3}He-^{4}He mixtures—in both the superfluid and the normal states—and investigations of convection in rotating layers of liquid helium.

CONTENTS

I. INTRODUCTION

This paper describes recent studies of Rayleigh-Bénard convection with particular emphasis on the experimental results which have been obtained using liquid helium. Rayleigh-Bénard convection occurs when a horizontal layer of fluid is heated from below with a sufficiently large heat flux to generate flow. The motivation for studying this system is twofold. From a practical viewpoint, many interesting processes involve thermally driven flows; among these are such diverse phenomena as convection in stars, the ocean, and the atmosphere, and the production of pure semiconductors. Normand, Pomeau, and Velarde (1977) have discussed a number of situations in which convection occurs. Additional reviews have been given by Busse (1978,1981) and Koschmieder (1974). From a fundamental point of view, convective flows provide experimentally realizable systems for very precise studies of nonlinear phenomena in dissipative systems; areas of study include the onset of turbulence and nonlinear pattern formation. An immense variety of systems, some of which have been recently discussed by Swinney (1983), fall within the rubric of nonlinear phenomena, and the availability of well-defined experiments is particularly important to theoretical progress.

Although Rayleigh-Bénard convection was studied early in this century by its namesakes, experimentally by Bénard (1901) and theoretically by Rayleigh (1916), the emergence of new techniques has provided comparably new and powerful insights. Specifically, lasers have provided precise local velocity data, computing power is greatly increased, and recent theoretical studies of nonlinear systems have provided an important framework for understanding the onset of turbulence. Cryogenic measurements, the focus of this paper, are particularly useful for obtaining exceptionally precise thermal information on the convecting and turbulent states. The relevant experimental parameters for normal (i.e., nonsuperfluid) liquid helium fall in a particularly fortunate range, as first pointed out by Ahlers (1974,1975). Despite the low temperatures involved, the cryogenic results are descriptive of flows in ambient air, yet they can be obtained with a precision greatly exceeding that obtainable with room-temperature gases. In addition, liquid helium offers a rich structure associated with the superfluid transition; here mixtures of the two stable isotopes ^{3}He and ^{4}He are particularly interesting.

An understanding of the phenomena involved in a convecting fluid requires a description of the equations of motion and an identification of the relevant parameters. Section II contains such a description, as well as a discus-

Copyright ©1985 The American Physical Society

sion of the thermodynamic, transport, and phase properties of liquid helium which make it such an unusual and useful fluid. At the end of the section there is a brief discussion of experimental considerations. Section III illustrates the current understanding of the laminar (i.e., steady) flows preceding turbulence using results drawn chiefly from cryogenic experiments. At this point, however, it is worth emphasizing that many room-temperature measurements involving flow visualization or direct velocity determinations have provided complementary information not available from the helium experiments. Any discussion of the cryogenic measurements requires a comparison to these other results. Section IV addresses the problem of turbulent onset. Only a brief review of recent theories pertaining to the route to turbulence is given, since more extensive theoretical discussions have been given by Ott (1981) and Eckmann (1981) and in *Order and Chaos* as introduced by Swinney (1983). It is important to note that this paper considers only the onset of turbulence or chaos and that fully developed turbulence lies outside its bounds. Examples drawn chiefly from low-temperature experiments demonstrate various aspects of theories describing the onset of chaos, and also show where more work is needed. Section V briefly describes several systems related to convection in a pure fluid that have been investigated using liquid helium. This section also reviews phenomena which are unique to the superfluid transition in mixtures of liquid ^{3}He and ^{4}He. Section VI provides a summary and an indication of possible new directions in cryogenic studies of convection and turbulence.

One additional point concerns the turbulence which occurs in pure ^{4}He in the superfluid phase. The turbulence in this case, arising from a tangle of quantized vortices, is distinctly different from that for a conventional Newtonian fluid. This area will not be considered here, but an extensive literature on superfluid turbulence exists, including a recent review by Tough (1982).

II. DESCRIBING RAYLEIGH-BÉNARD CONVECTION

A. Statement of the problem

The problem to be solved involves a layer of pure fluid shown schematically in Fig. 1(a), having uniform thickness d, and oriented in the direction perpendicular to gravity g. For definiteness, the coordinate origin is chosen so that the horizontal boundaries correspond to $z=\pm d/2$. On each boundary the temperature is fixed and independent of x or y. The expansion coefficient $\alpha_p=-\rho^{-1}(\partial\rho/\partial T)_p$ defined in terms of the mass density ρ is assumed positive throughout the fluid, and the bottom of the layer has a temperature ΔT warmer than the top. A complete hydrodynamic description gives the velocity $\mathbf{v}(\mathbf{r},t)$, the temperature $T(\mathbf{r},t)$, the pressure $P(\mathbf{r},t)$ throughout the fluid and for all times after $t=0$

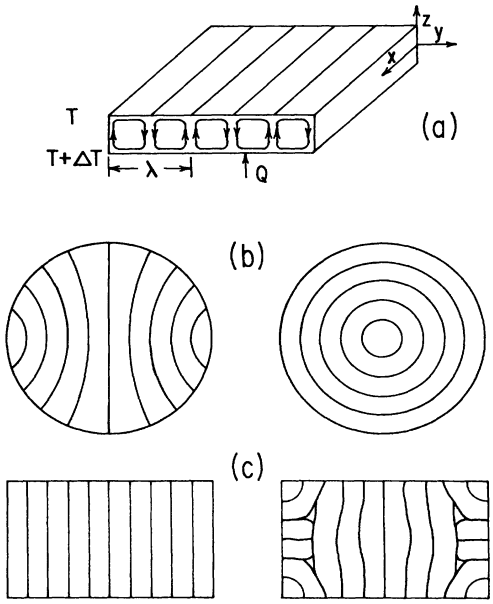

FIG. 1. (a) A layer of fluid having height d heated from below by a heat flux Q. (b) Schematic of possible patterns of convective rolls in a circulate container seen from above. (c) Schematic of possible patterns of convection rolls in a rectangular container also seen from above.

when initial values $\mathbf{v}(\mathbf{r},0)$, $T(\mathbf{r},0)$, $P(\mathbf{r},0)$ and boundary conditions are known.

B. Equations of motion

1. Conservation laws

The appropriate dynamics are inherently classical; the equations of motion in their most basic form are conservation laws [see, for instance, Landau and Lifshitz (1959)]. In principle, it might be necessary to consider microscopic degrees of freedom if the equations are to describe turbulence. Several theoretical (Zaitsev and Shliomis, 1970; Graham, 1974; Swift and Hohenberg, 1977) and experimental (Sano and Sawada, 1978; Ahlers, Cross, Hohenberg, and Safran, 1981) efforts have been directed toward understanding the effects of noise on Rayleigh-Bénard convection. However, both theory and experiment indicate that a continuum description suffices to describe convection near onset within current experimental resolution. One of the most important recent results is that the origins of turbulence in a convecting layer are usually attributable to the nonlinear interaction of macroscopic modes, not to microscopic fluctuations. The number of degrees of freedom needed to describe a turbulent convecting state may be relatively small, and the calculation of this number is an interesting problem which will be discussed briefly in Sec. IV.

The basic laws for mass, momentum, and energy conservation are, respectively,

$$\partial\rho/\partial t = -\nabla\cdot(\rho\mathbf{v}) , \tag{1}$$

$$\partial(\rho v_i)/\partial t = -\sum_k \partial\pi_{ik}/\partial x_k , \tag{2}$$

$$\partial(\tfrac{1}{2}\rho v^2+\rho\varepsilon+\rho gz)/\partial t$$

$$= -\nabla\cdot[\rho\mathbf{v}(\tfrac{1}{2}v^2+\varepsilon+gz+P/\rho)-\mathbf{v}\cdot\sigma-\kappa\nabla T] . \tag{3}$$

Here π_{ik}, the momentum flux density tensor, has components

$$\pi_{ik} = P\delta_{ik}+\rho v_i v_k+\sigma_{ik} , \tag{4}$$

with the viscous stress tensor σ_{ik} given by

$$\sigma_{ik} = \eta(\partial v_i/\partial x_k+\partial v_k/\partial x_i-\tfrac{2}{3}\delta_{ik}\nabla\cdot\mathbf{v})+\zeta\delta_{ik}\nabla\cdot\mathbf{v} . \tag{5}$$

Other quantities introduced in these equations are ε, the internal energy per mass, η, the shear viscosity, ζ, the bulk viscosity, and κ, the thermal conductivity. All of these depend on the independent thermodynamic variables T and P, which may vary in space and time.

Alternative formulations of both Eqs. (2) and (3) are more conventional. From Eqs. (1) and (2) the time variation of $\mathbf{v}$ is given by

$$\rho[\partial\mathbf{v}/\partial t+(\mathbf{v}\cdot\nabla)]\mathbf{v} = -\nabla P+\rho\mathbf{g}+\eta\nabla^2\mathbf{v} +(\zeta+\eta/3)\nabla(\nabla\cdot\mathbf{v}) . \tag{6}$$

Inherent in Eq. (6) is the assumption that η and ζ are effectively uniform throughout the fluid. Since both quantities depend on T and P, this assumption, although usually valid, requires justification.

A more conventional formulation of Eq. (3) occurs by identifying the reversible and irreversible contributions to the energy transport. The reversible contributions can be removed through Eqs. (1) and (2) and the remaining irreversible terms form the entropy equation given for s, the entropy per mass:

$$T(\partial s/\partial t+\mathbf{v}\cdot\nabla s) = \nabla\cdot(\kappa\nabla T)+\tfrac{1}{2}\eta\sum_k(\partial v_i/\partial x_k+v_k/\partial x_i-\tfrac{2}{3}\delta_{ik}\nabla\cdot\mathbf{v})^2+\zeta(\nabla\cdot\mathbf{v})^2 . \tag{7}$$

Near the onset of convection, several approximations are in order. The density of parcel of fluid is nearly constant as it moves about—i.e., to a good approximation

$$d\rho/dt = \partial\rho/\partial t+\mathbf{v}\cdot\nabla\rho = 0 , \tag{8}$$

or the fluid is incompressible. As a consequence, Eq. (1) becomes

$$\nabla\cdot\mathbf{v} = 0 , \tag{9}$$

and Eq. (6) becomes the Navier-Stokes equations

$$\rho[\partial\mathbf{v}/\partial t+(\mathbf{v}\cdot\nabla)\mathbf{v}] = -\nabla P+\rho\mathbf{g}+\eta\nabla^2\mathbf{v} . \tag{10}$$

Since the flows are buoyancy driven and not pressure driven, $s(P,T)$, in Eq. (7) depends relatively little on P. Likewise, the pressure dependence of $\rho(P,T)$ in Eq. (10) is relatively unimportant. If the temperature gradients are not too large, then these quantities can be approximated as

$$\rho = \rho_0[1-\alpha_p(T-T_0)] , \tag{11a}$$

$$s = s_0+c_p(T-T_0)/T_0 . \tag{11b}$$

The quantities ρ_0, T_0, and s_0 are constants corresponding to appropriate values within the layer, and c_p is the specific heat per mass. The approximation of Eq. (11a) is used for the body force term $\rho\mathbf{g}$ in Eq. (10); otherwise, ρ can be treated as a constant equal to ρ_0. Note that the dependence of ρ on T must be included in the body force to describe convection. The terms multiplied by η in Eq. (7) are negligible compared to others in the equation, at least when the flow is near onset. In addition, the thermal conductivity is generally nearly constant over the layer. Implementing these approximations in Eq. (7) yields the heat equation:

$$\partial T/\partial t+\mathbf{v}\cdot\nabla T = D_T\nabla^2 T , \tag{12}$$

where D_T is the thermal diffusivity defined by $D_T=\kappa/\rho c_p$.

Equations (9)–(12), known as the Oberbeck (1879)-Boussinesq (1903) approximation, form the springboard for further discussion. The approximations mentioned above are discussed in more detail by Gray and Giorgini (1976) among others. Nevertheless, the nonlinear terms $(\mathbf{v}\cdot\nabla)\mathbf{v}$ in Eq. (10) and $\mathbf{v}\cdot\nabla T$ in Eq. (12) are thought to be the most important nonlinear terms for the convective problem. Their presence is responsible for a number of interesting effects, including turbulence. In particular, because these terms are nonlinear, they allow the possibility of multiple solutions, in an analogous way to the multiple roots which occur in nonlinear algebraic equations.

2. Equations of motion in dimensionless form

A useful formulation, as discussed by Schlüter, Lortz, and Busse (1965) is produced by rescaling the variables of Eqs. (9)–(12) in terms of natural units for the system; in this manner, the resulting dimensionless equations contain only two dimensionless parameters instead of a much larger number of dimensioned ones. The natural units are put together from the various quantities $D_T,\eta,\ldots$. A useful although not unique convention expresses length, time, mass, and temperature in units of d, d^2/D_T, $\rho_0 d^3$, and $D_T\nu/\alpha_p g d^3$. Here $\nu=\eta/\rho$ is the kinetic viscosity. The quantity $d^2/D_T\equiv t_v$ is particularly useful; it corresponds roughly to the time for heat to diffuse vertically across the layer. It is also useful to write the temperature field, still in dimensioned units, as the sum of a steady

conductive portion $-(\Delta T/d)z$ and a convective portion θ:

$$T(r,t)=T(0)-\Delta Tz/d+\theta(\mathbf{r},t)\ . \tag{13}$$

Note that below the onset of convection, $\theta=0$ in the steady state. Using the new temperature representation and then expressing all quantities in terms of natural units, we see that the equations of motion become

$$\nabla\cdot\mathbf{v}=0\ , \tag{14}$$

$$\partial\mathbf{v}/\partial t+(\mathbf{v}\cdot\nabla)\mathbf{v}=-\nabla w+\mathrm{Pr}\theta\hat{z}+\mathrm{Pr}\nabla^2\mathbf{v}\ , \tag{15}$$

$$\partial\theta/\partial t+\mathbf{v}\cdot\nabla\theta=R\hat{z}\cdot\mathbf{v}+\nabla^2\theta\ , \tag{16}$$

where w contains a dimensionless pressure term as well as terms generated by using Eq. (13) in the Navier-Stokes equations. Equations (14)—(16) contain only the dimensionless parameters R, the Rayleigh number, and Pr, the Prandtl number:

$$R=\alpha_p g d^3\Delta T/D_T\nu \tag{17}$$

and

$$\mathrm{Pr}=\nu/D_T\ . \tag{18}$$

Qualitatively, R provides a measure of the competition between buoyancy and dissipation, with $\alpha_p g\Delta T$ giving a measure of the former, and νD_T giving a measure of the latter. The appearance of both ν and D_T is understandable, since a rising volume of warm fluid loses energy by viscous drag and by thermal diffusion to the colder surroundings. Convection begins at a nonzero critical Rayleigh number R_c when the available buoyancy overcomes the effects of dissipation. For a horizontally infinite layer, this happens for $R_c=1707.76\ldots$. Real experiments must be done in finite geometries having vertical walls which exert additional drag on the fluid. Consequently, horizontally confined layers have values of R_c greater than 1707.8, although the effect is small as long as the horizontal dimension of the layer is large compared to d. Convection begins in the form of rolls with alternating upward and downward flow which in ideal cases may resemble those in Fig. 1(a). In actual experiments the arrangement of the rolls may resemble some of the less ordered patterns shown schematically in Figs. 1(b) and 1(c). The roll pattern wavelength, λ, is of order $2d$, a fact which can be qualitatively understood in simple terms: if λ is too large, the viscous drag from the horizontal boundaries will inhibit the flow, if λ is too small, upward-welling warm fluid will both be able to easily lose heat to nearby falling liquid and experience increased viscous drag. Consequently, when convection begins in a very wide layer, the dimensionless wave number α,

$$\alpha=2\pi d/\lambda \tag{19}$$

is predicted (Chandrasekhar, 1961) to have the critical value $\alpha_c=3.117\ldots$, or $\lambda/d=2.02\ldots$.

The parameter Pr gives a relative measure of viscous and thermal diffusion; values of Pr for some fluids are listed in Table I. Fluids with similar Prandtl numbers, such as air and liquid helium, are expected to behave similarly, although a comparison of the dimensioned parameters would not lead to such an unexpected conclusion. In addition, experimentally obtainable liquid-helium Prandtl numbers extend close to values which are easily obtainable with water. Thus helium forms at least a partial bridge between common fluids like water and very low Prandtl number fluids like liquid metals, typified by mercury.

TABLE I. Some typical Prandtl numbers.

Fluid	Pr
Air	0.7
Liquid helium	0.5—1.0
Mercury	0.025
Oils	10 and greater
Water	2—10

One last parameter concerns the effect of vertical containing walls. Since heat transfer and some stretching or squeezing of the convection rolls occur due to these walls, their effect is important. This is particularly true when the horizontal dimension of the layer is comparable to the height d. An obviously important parameter is the ratio of an appropriate horizontal length X to the height d, a quantity called the aspect ratio Γ:

$$\Gamma\equiv X/d\ . \tag{20}$$

The characteristic length X must be chosen for each shape of the sidewalls. Although there are no unique choices, a useful convention is to choose X for a given geometry so that Γ roughly represents the number of pairs of convection rolls. For a cylindrical geometry which may have either axisymmetric rolls or roughly parallel rolls, as sketched (from above) in Fig. 1(b), a good choice for X is the radius, which for reasons of clarity we write as $\mathscr{D}/2$, with $\mathscr{D}$ the diameter. Then

$$\Gamma=\mathscr{D}/2d\ \ \text{(cylinders)}\ . \tag{21}$$

For rectangles a complete description gives both the length and width in units of d. Under carefully prepared initial conditions, the rolls will align parallel to the short side of the rectangle, but for random initial conditions, patterns with defects will form. Hypothetical examples are sketched in Fig. 1(c). As discussed in Sec. IV, the aspect ratio plays a critical role in the evolution of turbulence. In particular, the turbulent states arising in small-Γ containers with their constrained rolls are expected to be rather different from those in large-Γ containers, where the flow pattern can make adjustments with considerably more freedom.

C. Fluid parameters and experimental considerations

1. Pure helium

Liquid helium has a number of interesting characteristics which in combination allow the experimenter an exceptional degree of flexibility and precision. Extensive re-

views dealing with the properties of helium are given by Wilks (1967) and Ahlers (1976), and tabulations of data have been compiled by Hill and Lounasmaa (1960), Barenghi, Lucas, and Donnelly (1981), and Behringer and Ahlers (1982). Due to their quantum nature both ^{4}He and ^{3}He show features which differ from those of most other fluids. Both liquefy only at low temperatures; ^{4}He has a critical temperature of 5.2 K, and ^{3}He has a critical temperature of 3.3 K. Both undergo an additional transition to a superfluid state. ^{4}He is the most extensively used working fluid in cryogenic convection experiments; its phase diagram appears in Fig. 2. The boundary between normal and superfluid, called the lambda line, terminates at the saturated vapor pressure curve when $T=2.172$ K. Continuing upward with a negative slope, this boundary intersects the melting curve at 1.763 K. To the right of the lambda line, ^{4}He behaves like a classical or normal fluid, and the ^{4}He experiments described in this paper are performed in this region. Near the superfluid transition and at slightly warmer temperatures runs a curve along which the expansion coefficient α_p vanishes; in a region to the left of the curve the expansion coefficient is negative. A parallel situation occurs for water at 4 °C, and interesting convective phenomena occur in the neighborhood of vanishing α_p. The superfluid transition and the critical point, terminating the saturated vapor pressure curve, are responsible for many of the interesting properties which characterize ^{4}He. In particular, at these transitions, the thermal conductivity κ is divergent; for the intervening temperatures, κ remains large, due to the presence of the transitions. Figure 3(a) gives κ for ^{4}He at saturated vapor pressure. Using data from White (1959) for comparison, we see that two useful metals, stainless steel and oxygen-free high-conductivity (OFHC) copper, have conductivities of $\sim$0.002 W/cm K and $\sim$4 W/cm K in the temperature range of interest. Inspection of Fig. 3 provides an understanding of the reason precise thermal measurements can be made using liquid helium. To obtain a system which closely matches the idealized problem of uniform temperatures at the horizontal boundaries, the experimenter needs a solid material with a high conductivity compared to the fluid. OFHC copper clearly satisfies that requirement. On the other hand, if the vertical walls are too-efficient thermal conductors, the effect of the fluid will be lost. Often helium measurements are made with very thin stainless-steel walls which divert only $\sim$20% of the heat flux away from the fluid. In addition, the transfer of energy by radiation is insignificant in cryogenic experiments, but a serious problem is room-temperature experiments.

One of the most important aspects of the cryogenic measurements is their capability of producing information on time-dependent flows by heat flux or temperature measurements. If large thermal masses surround the fluid, temperature oscillations may be severely attenuated before reaching a detector. Due to the fact that the specific heat of helium [Fig. 3(b)] is very large compared

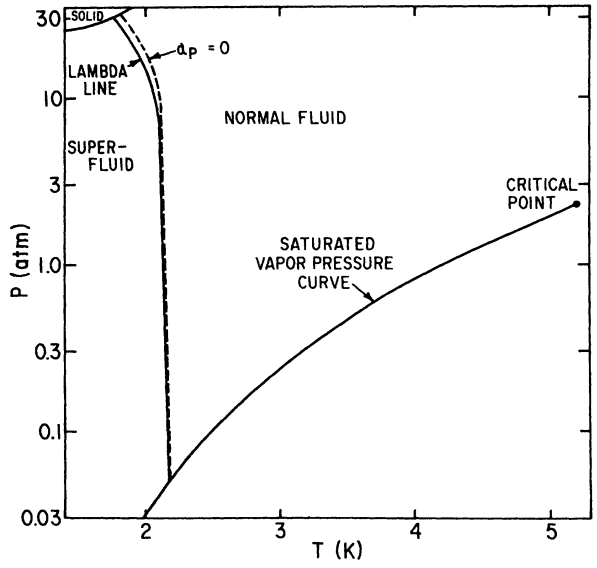

FIG. 2. Phase diagram of ^{4}He showing the superfluid or lambda line, the line along which the isobaric expansion coefficient $\alpha_p=0$, and the saturated vapor pressure curve where most convection measurements have been made. To the right of the lambda line liquid helium is a conventional Newtonian fluid.

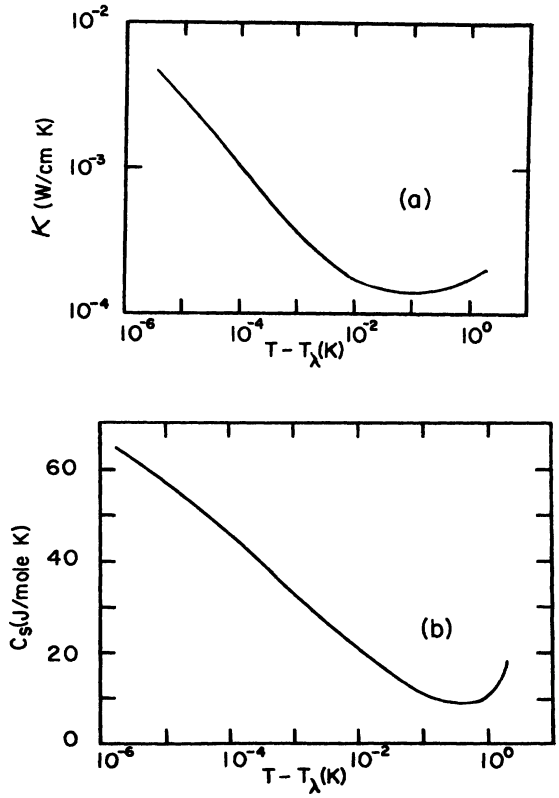

FIG. 3. (a) The thermal conductivity κ of liquid helium at saturated vapor pressure vs temperature. (b) The specific heat C_s of liquid helium at saturated vapor pressure vs temperature. C_s differs from the specific heat at constant pressure Cp by a small correction. These curves are from data fitted by Barenghi, Lucas, and Donnelly (1981), and include work by Ahlers (1968), Ahlers and Behringer (1979), Buckingham and Fairbank (1961), Keller (1969), and Hill and Lounasmaa (1957).

to the small (~ 0.002 J/cm^{3}K) specific heats of a metal such as copper which also has a very high thermal conductivity, thermal signals can propagate from the fluid to a thermometer with virtually no attention. A well-defined criterion for the experimental quality of the horizontal boundaries is based on the following simple argument (Behringer *et al.*, 1980). A fluctuation $\delta T e^{-i\omega t}$ in the temperature at, say, the bottom of the fluid must propagate through a thickness h of the bounding material to reach a thermometer. Because the signal propagates by thermal diffusion, it is attenuated. The ratio of the received to the transmitted power is easily calculated to be

$$H(\omega)=2[\cosh(\omega/\omega_0)^{1/2}+\cos(\omega/\omega_0)^{1/2}]^{-1}, \quad (22)$$

where $\omega_0=D_b/2h^2$ and D_b is the thermal diffusivity of the boundary. Frequencies above ω_0 are attenuated exponentially. In a typical helium experiment the fastest frequencies satisfy $\omega/\omega_0<0.01$, well within a safe limit.

The cryogenic measurements exploit existing technology for making very precise measurements at low temperatures. Using resistance thermometry techniques discussed by Mueller, Ahlers, and Pobell (1976), and Behringer and Ahlers (1982), one can resolve temperature changes of ~ 0.1 μK. This resolution is very small compared to a typical value, $\Delta T_c \sim 1$ mK, for ΔT at R_c. The exact size of ΔT_c depends on the thermohydrodynamic properties α_p, D_T, ν, all of which vary with the mean temperature of the layer, as well as the acceleration of gravity g, d, and the geometry of the container. In a typical experiment for a large aspect-ratio layer using liquid helium at saturated vapor pressure, with $d=0.1$ cm, the values of ΔT_c depend on the mean temperature as shown in Fig. 4(a). Over a significant temperature range the experimental resolution in this case is at least 0.1% of ΔT_c and often better. By using containers of differing heights, an experimenter can always optimize the resolution.

An additional consideration is the extent to which the helium satisfies the Oberbeck-Boussinesq approximation. In particular, when ΔT_c becomes large, the temperature dependence of the fluid parameters may no longer be negligible. Busse (1967b) has investigated this problem theoretically, and Ahlers (1980b) and Walden and Ahlers (1981) have studied it experimentally. The relevant parameter describing departures from the Oberbeck-Boussinesq (OB) approximation is

$$Q_{\rm OB}=\sum_i \gamma_i P_i , \quad (23)$$

where the γ_i's are a factor of ΔT times, respectively, the logarithmic temperature derivatives of ρ^{-1}, $|\alpha_p|^{1/2}$, ν, κ, and c_p. The P_i's are Prandtl number dependent, but otherwise constant. The flow is Boussinesq for $|Q_{\rm OB}| \ll 1$. Figure 4(b) shows $Q_{\rm OB}$, evaluated at ΔT_c, versus temperature as calculated for helium layers with $d=0.1$ cm. Over much of the experimental range $|Q_{\rm OB}| \lesssim 0.02$, which is a quite reasonable value.

Although experiments are usually designed to satisfy the Oberbeck-Boussinesq approximation fairly well, departures from this approximation are also interesting.

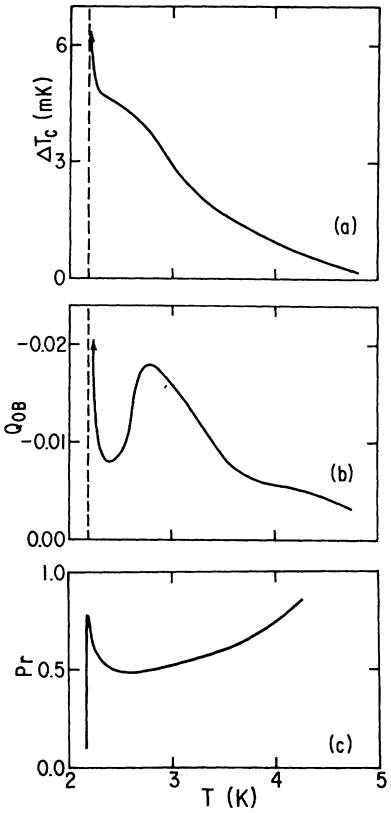

FIG. 4. (a) The temperature difference ΔT_c at the onset of convection for a 0.1-cm-high layer of liquid helium at saturated vapor pressure as a function of the mean temperature T. (b) The parameter $Q_{\rm OB}$ vs mean operating temperature T for the values of ΔT_c given in (a). $Q_{\rm OB}$ is defined by Eq. (23) and measures the departure from the Oberbeck-Boussinesq approximation. (c) The Prandtl number Pr as a function of T for liquid helium at saturated vapor pressure.

Recently cryogenic studies dealing with nonideal convection have been made by Ahlers (1975,1980b) and by Walden and Ahlers (1981). The latter have examined the phenomena of penetrative convection, a topic which has been studied theoretically by Moore and Weiss (1973) and Musman (1968). Penetrative convection occurs for fluids such as liquid helium having a temperature range over which the expansion coefficient, α_p, is negative. The phenomenon is induced by adjusting the cold top temperature to be in the region $\alpha_p<0$ and the hot bottom temperature in the region $\alpha_p>0$. Only the bottom of the layer is gravitationally unstable. However, when convection begins, flow in the unstable part induces flow in the stable part, hence the name *penetrative convection.* A number of interesting phenomena occur in this and other non-Boussinesq situations, including the formation of cellular flow patterns.

Figure 4(c) [after Barenghi *et al.* (1981)] shows an additional property of interest, the Prandtl number of liquid helium at saturated vapor pressure as a function of temperature.

One final point should be made regarding experimental procedure. In nearly all cryogenic experiments, the heat flux Q is the fixed parameter rather than ΔT, the fixed parameter of theoretical calculations. In addition, the temperature at the top of the layer is held fixed. The reason for fixing Q rather than ΔT is the increased resolution usually available by this technique. For steady flows, i.e., those for which $\partial \mathbf{v}/\partial t = \partial T/\partial t = 0$, the distinction is usually not important. However, as argued by Busse (1967a), the distinction may be important for time-dependent flows. Evidence presented by Gao and Behringer (1984) indicates that fixing Q rather than ΔT does not seriously affect the time-dependent flows near the onset of turbulence in liquid-helium experiments.

2. Mixtures of ^{3}He and ^{4}He

The precise techniques which make pure helium an excellent experimental medium also apply to mixtures of ^{3}He and ^{4}He. When X, the molar concentration of ^{3}He, is gradually increased from zero, the superfluid transition temperature is depressed. This is demonstrated in Fig. 5, which gives the T-X phase diagram at saturated vapor pressure. When X is sufficiently large, $X > 0.675$, the continuous superfluid transition is altered to a first-order transition in which the liquid separates into two distinct phases of different isotopic composition and density. Separating the first-order transition curves and the lambda line is a tricritical point. The relevant thermohydrodynamic coefficients, discussed in Sec. V, vary significantly from one section of the phase diagram to another, giving the experimenter an exceptionally broad parameter range for studying the properties of mixtures. Also discussed in Sec. V are the unique convective flows occurring in superfluid ^{3}He-^{4}He mixtures.

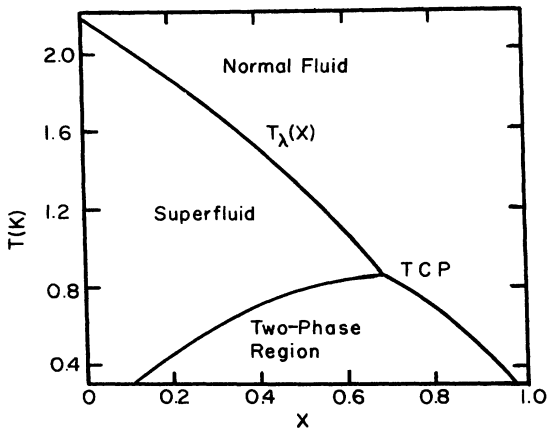

FIG. 5. The phase diagram in the T-X plane for ^{3}He-^{4}He mixtures at saturated vapor pressure. Relevant features include the superfluid or lambda transition, $T_\lambda(X)$, the tricritical point (TCP), and the two-phase region bounded by the first-order transition lines.

III. STEADY FLOWS IN A PURE FLUID

A. Introduction

The steady or laminar flows preceding turbulence are interesting for several reasons. Since they precede turbulent flows, any detailed description of turbulence should consider their nature. In this regard, linear stability theory, which predicts the onset of instabilities of a steady state to small perturbations is particularly pertinent. In turn, linear stability theory for convective flows is paralleled by similar analyses in a variety of problems. Finally, the laminar flows are also interesting in their own right, and the evolution of a steady flow described by nonlinear dynamics is a challenging problem.

B. Transition to convection

The transition to convection in a horizontally infinite layer provides a simple example of stability theory, and a foundation for further discussion of convective flows. Here the discussion will be fairly brief, but a detailed discussion is given in Chandrasekhar (1961).

Stability theory begins by finding a steady solution, which for $R < R_c$ corresponds to $\mathbf{v} = \theta = 0$. Then the dimensionless temperature field T for the steady solution satisfies $\nabla^2 T = 0$, so that

$$T - T_0 = -Rz \ . \tag{24}$$

Also, by inspection of Eq. (15), the effective pressure term w must then be a constant.

Finding a steady solution does not complete the problem, however, since there may exist other steady solutions. In order to be relevant, a solution must also be stable. Here there are two types of stability. The weakest is local stability, a term referring to the response of the system to an arbitrary infinitesimal perturbation. If all possible infinitesimal perturbations on the steady state decay in time, then the solution is locally stable. The stronger type of stability, global stability, is inherently more difficult to prove and considers the response of the system to any size perturbation.

Continuing with the convective onset as an example of local stability, we find that the next procedure in the calculation is a search for solutions consisting of the laminar state with a superposed infinitesimal perturbation. Due to their smallness all terms higher than linear order in the perturbation are neglected. In the present example, θ and $\mathbf{v}$ are both considered to be infinitesimals, which in this case will be written as $\delta\theta$ and $\delta\mathbf{v}$ to emphasize that condition. The pressure term w has the form $w = \text{const} + \delta w$. The fields $\delta\mathbf{v}$, $\delta\theta$, and δw are assumed to have the space-time separated forms

$$\delta \mathbf{v} = \mathbf{V}(\mathbf{r}) e^{\sigma t} \ , \tag{25}$$

$$\delta\theta = \Theta(\mathbf{r}) e^{\sigma t} \ , \tag{26}$$

$$\delta w = W(\mathbf{r}) e^{\sigma t} \ . \tag{27}$$

The resulting linearized equations for these modes are

$$\nabla\cdot\mathbf{V}=0\ , \tag{28}$$

$$\sigma\mathbf{V}=-\nabla W+\mathrm{Pr}\Theta\hat{z}+\mathrm{Pr}\nabla^2\mathbf{V}\ , \tag{29}$$

$$\sigma\Theta=RV_z+\nabla^2\Theta\ . \tag{30}$$

When the appropriate boundary conditions are invoked, the result is a self-adjoint eigenvalue problem for the growth rate σ. If all the eigenvalues, which must be real, are negative, the steady solution is stable; otherwise, it is unstable to any mode with positive σ.

In the case at hand one obvious type of mode has $\mathbf{V}=\mathbf{0}$, $\Theta=\Theta(z)$, so that Θ corresponds to a solution of Fourier's law. This sort of diffusive mode, which is observed experimentally below the onset of convection, often has the form

$$\Theta=\sin[q_n(z-\tfrac{1}{2})]\ , \tag{31}$$

$$q_n=(2n+1)\pi/2,\quad n=0,1\ldots, \tag{32a}$$

$$\sigma_n=-q_n^2<0\ . \tag{32b}$$

The values of q are quantized, since $\Theta=0$ at $z=\frac{1}{2}$, and the heat flux $\partial\Theta/\partial z=0$ at $z=-\frac{1}{2}$. These conditions must be invoked if the usual experimental conditions of fixed heat flux and fixed top temperature are to be valid.

When R (or ΔT) is small enough, these slowest one-dimensional diffusive modes relax the slowest in response to a transient, and therefore dominate for long times. As R grows, buoyancy becomes more important. The system moves closer to being able to sustain convection, and consequently the convective modes to be described below will tend to decay more slowly. At the onset of convection the critical mode neither grows nor decays; when R exceeds R_c, this mode will grow exponentially until the discarded nonlinear terms become important.

The convection modes can be obtained by operating on Eq. (29) with $\nabla\times\nabla\times$ and taking the z component. This leaves only V_z and Θ coupled via Eq. (30) and

$$\sigma\nabla^2V_z=\mathrm{Pr}(\nabla^2-\partial^2/\partial z^2)+\mathrm{Pr}(\nabla^2)^2V_z\ . \tag{33}$$

When describing a laterally infinite layer, one makes the difference between the horizontal and vertical directions explicit by looking for solutions having a spatial dependence $e^{i\boldsymbol{\alpha}\cdot\mathbf{r}}e^{qz}$. Here

$$\alpha=(\alpha_x,\alpha_y,0) \tag{34}$$

is the horizontal wave vector, with the value of α determining the value of the convective wavelength λ. Equations (30) and (33) lead to the characteristic equation

$$(q^2-\alpha^2)[(\sigma/\mathrm{Pr})-(q^2-\alpha^2)][\sigma-(q^2-\alpha^2)]=-R\alpha^2 \tag{35}$$

linking α, R, σ, Pr, and q with the additional constraint

$$V_z/\Theta=(\sigma+\alpha^2-q^2)/R\ . \tag{36}$$

In order to complete the problem, one must impose the relevant boundary conditions. These are assumed to be "rigid" boundary conditions with $\mathbf{v}=0$, $\theta=0$ on the horizontal surfaces. Using these conditions with $\nabla\cdot\mathbf{v}=0$ leads to the restrictions

$$V_z=\partial V_z/\partial z=\Theta=0\quad(z=\pm\tfrac{1}{2})\ . \tag{37}$$

When R, P, α, and σ are given, Eq. (35) yields six values for q, allowing a superposition of six terms each for Θ and V_z in the various terms $e^{-i\boldsymbol{\alpha}\cdot\mathbf{r}}e^{qz}$. The six relations of Eqs. (37) imply a functional relationship

$$\sigma=\sigma(R,\mathrm{Pr},\alpha)\ . \tag{38}$$

The most important case occurs for $\sigma=0$. Then the allowed values $R(\alpha)$ form the boundary above which the convective modes will begin to grow in linear order and the conductive solution will be unstable. It is important to note that when $\sigma=0$, a condition known as neutral stability, the Prandtl number dependence contained in Eq. (35) vanishes; consequently the onset value R for a given mode depends only on α. Figure 6 shows the resulting neutral stability curve R vs α for the lowest symmetric mode, which is the one for which convection can first begin. The smallest or critical Rayleigh number of the neutral stability curve, R_c, and corresponding critical value of α are

$$R_c=1707.76\ , \tag{39}$$

$$\alpha_c=3.117\ . \tag{40}$$

That $\alpha_c=3.117$ clearly corresponds to rolls only slightly wider than they are high.

When R is just larger than R_c, other modes with wave vectors near α_c will also grow in the linear theory, and the conductive solution will be unstable over a continuum of wave vectors, with any orientation also allowed for the convective rolls. The growth rates and onset Rayleigh numbers for these near-critical modes can be obtained by expanding Eq. (38). The relevant derivatives which are evaluated at $\alpha=\alpha_c$, $R=R_c$ are given by Wesfreid *et al.* (1978) and for Eq. (41) by Behringer and Ahlers (1977):

$$\tau_0^{-1}\equiv R_c\,d\sigma/dR=38.40\mathrm{Pr}/(1+1.954\mathrm{Pr})^{-1}\ , \tag{41}$$

and

$$\xi_0^2=(2R_c)^{-1}d^2R/d\alpha^2=0.3848\ . \tag{42}$$

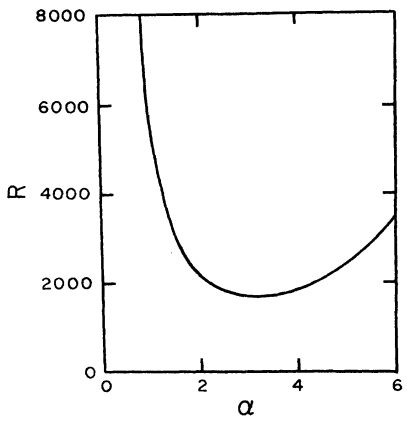

FIG. 6. The neutral stability curve R vs α for a horizontally infinite layer of fluid. See Chandrasekhar (1961).

The relation giving σ for near-critical modes is then

$$\sigma=\tau_0^{-1}[(R-R_c)/R_c-\xi_0^2(\alpha-a_c)^2] . \quad (43)$$

This relation indicates that the growth rate σ for the critical mode ($\alpha=\alpha_c$) will linearly increase from negative to positive values as R increases from a subcritical to a supercritical value. Also, modes having $\alpha\neq\alpha_c$ will have growth rates which are reduced by the quadratic term $(\alpha-\alpha_c)^2$.

So far, the effects of the vertical boundaries have been neglected. When Γ is very large, the infinite—aspect-ratio approximation is reasonable, at least in determining R_c. However, as Γ decreases, the vertical walls exert extra drag on the fluid which must be overcome by the buoyancy force for convection to begin. Consequently $R_c(\Gamma)$ will increase as Γ decreases. Although this is conceptually clear, obtaining a numerical result for R_c becomes considerably more difficult. Solutions with the exponential time dependence $e^{\sigma t}$ are still possible, but attempts to find solutions which are separable in the horizontal and vertical directions and which simultaneously satisfy rigid boundary conditions on all the surfaces are unsuccessful; the wave number α is no longer a sharply determined parameter. However, values of R_c can be obtained by a Rayleigh-Ritz technique, since the eigenvalue problem corresponds to a self-adjoint operator with the quantity R_u defined for volume integrals over the entire layer,

$$R_u=\frac{\int\Theta\nabla^2\Theta\,d^3r}{\int(\mathbf{V}\cdot\nabla^2\mathbf{V}+2\Theta V_z)d^3r} , \quad (44)$$

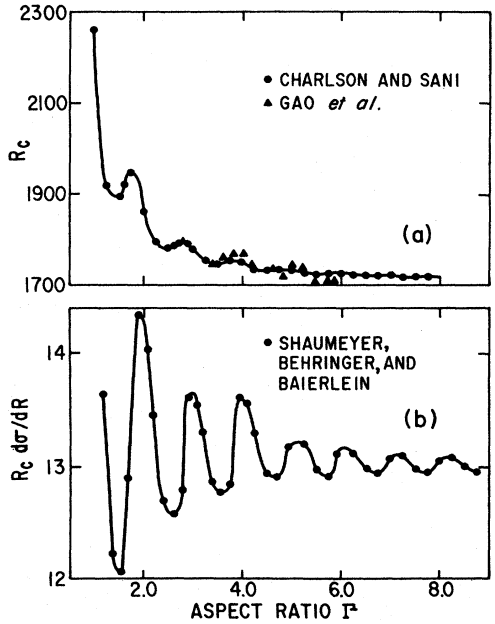

FIG. 7. (a) Critical Rayleigh numbers R_c (Charlson and Sani, 1970) and (b) growth rate derivative $R_c d\sigma/dR$ vs aspect ratio, for axisymmetric modes in cylindrical containers with insulating sidewalls (Shaumeyer, Behringer, and Baierlein, 1981). The triangles in (a) are experimental data from Gao, Metcalfe, Jung, and Behringer (1985).

providing an upper bound to R_c. Charlson and Sani (1970,1971) have used such a technique to obtain estimates for R_c in containers with cylindrical geometry. The form which they use to obtain R_u differs from Eq. (44) due to their choice of nondimensionalizing factors. These calculations are useful in cryogenic measurements, many of which have been made with cylindrical containers. Figure 7(a) shows values of R_c vs Γ as calculated by Charlson and Sani for axisymmetric modes and insulating side walls. Although nonaxisymmetric modes may have somewhat smaller values of R_c for some values of Γ, the results of Fig. 7(a) lead to the qualitatively correct conclusion that vertical walls affect R_c only for $\Gamma\lesssim 2$. Gao, Metcalfe, Jung, and Behringer (1985) have measured $R_c(\Gamma)$ in the range $3\lesssim\Gamma\lesssim 6$ using liquid ^{4}He in cylindrical containers. The results, shown as triangles in Fig. 7(a), agree rather well with the theoretical calculations for axisymmetric modes. An extension of the Rayleigh-Ritz technique for calculating $d\sigma/dR$ has been used by Shaumeyer, Behringer, and Baierlein (1981) to show that this quantity also varies little from the infinite-layer value unless the aspect ratio satisfies $\Gamma\lesssim 2$. Their results for insulating sidewalls and axisymmetric modes are shown in Fig. 7(b).

C. Convection just above R_c

The steady flows which evolve for $R>R_c$ are more difficult to describe, since they require nonlinear terms which were discarded in the stability analysis for the onset of convection. These nonlinear terms cause the critical or near-critical modes, which initially grow exponentially, to approach a saturated steady value. In addition, they allow more than one steady solution, so that the theory should also determine which solutions are stable. Schlüter, Lortz, and Busse (1965) have carried out a detailed analysis of the steady solutions applicable for $R\gtrsim R_c$ and an infinite horizontal layer. Adapting their notation, one can write the complete equations of motion (14)—(16) as

$$\partial\bar{u}/\partial t+(\bar{u}\cdot\bar{\partial})\bar{u}=\mathbf{D}\,\bar{u}-\bar{\partial}w , \quad (45)$$

with

$$\bar{\partial}\cdot\bar{u}=0 . \quad (46)$$

Here $\bar{u}$ is a four-component column vector field

$$\bar{u}=(u_0,u_1,u_2,u_3)^T=(\theta,v_x,v_y,v_z)^T ,$$

$\mathbf{D}$ is a matrix operator

$$\mathbf{D}=\begin{bmatrix}\nabla^2 & 0 & 0 & R\\ 0 & \mathrm{Pr}\nabla^2 & 0 & 0\\ 0 & 0 & \mathrm{Pr}\nabla^2 & 0\\ \mathrm{Pr} & 0 & 0 & \mathrm{Pr}\nabla^2\end{bmatrix} , \quad (47)$$

and $\bar{\partial}$ is the four-dimensional operator $\bar{\partial}=(0,\partial/\partial x,\partial/\partial y,\partial/\partial z)$. $\mathbf{D}$ has the interesting property of being self-adjoint with respect to the scalar product defined in terms of the total volume integrals over the fluid

$$\langle \bar{u},\bar{u}' \rangle = R \int (u_1^* u_1' + u_2^* u_2' + u_3^* u_3') d^3r + \mathrm{Pr} \int u_0^* u_0' d^3r \quad (48)$$

for two four vectors $\bar{u},\bar{u}'$ whose components satisfy Eq. (46) and rigid boundary conditions. Indeed, the linear stability problem for the onset of convection results when the term $(\bar{u}\cdot\bar{\partial})\bar{u}$ is omitted from Eq. (45) and only **D** remains. That **D** is a self-adjoint follows from the choice of the metric factors R and Pr in (48), from the fact that only ∇^2 appears in the differential components of **D**, from the boundary conditions imposed on the fields $\bar{u}$ and $\bar{u}'$, and from the condition $\bar{\partial}\cdot\bar{u}=0$.

Schlüter, Lortz, and Busse obtained steady (i.e., time-independent) solutions to Eqs. (45) and (46) and investigated their stability by means of an expansion in a small parameter λ, which gives a measure of how far the system is above R_c. Since **v**, θ, and $R-R_c$ vanish at the critical Rayleigh number, the expansion takes the form

$$R - R_c = \lambda R^{(1)} + \lambda^2 R^{(2)} + \cdots , \quad (49)$$

$$\bar{u} = \lambda \bar{u}^{(1)} + \lambda^2 \bar{u}^{(2)} + \cdots . \quad (50)$$

One of the key results of this analysis is that $R^{(1)}$ vanishes, so that to leading order

$$\lambda \propto (R - R_c)^{1/2} . \quad (51)$$

As a consequence, v and θ vary as $(R-R_c)^{1/2}$ near R_c. Figure 8 shows an experimental confirmation of this result due to Bergé and Dubois (1974) and Bergé (1975). Here one component of **v**, at a fixed position in the layer, as measured using a laser velocimetry technique, is shown versus

$$\varepsilon \equiv (R - R_c)/R_c . \quad (52)$$

The data agree quite well with the solid line which varies as $\varepsilon^{1/2}$.

In the case of liquid-helium measurements, the velocity field is not readily observable. However, the dimensionless heat flux **Q** is simply related to the dimensionless velocity and temperature by

$$\mathbf{Q} = -\nabla T + T\mathbf{v} . \quad (53)$$

In the steady state, the total heat per area per time carried from the bottom to the top of the layer is identical to the volume average $\langle Q_z \rangle$ of the vertical component of **Q**:

$$\langle Q_z \rangle = R + \langle \theta v_z \rangle . \quad (54)$$

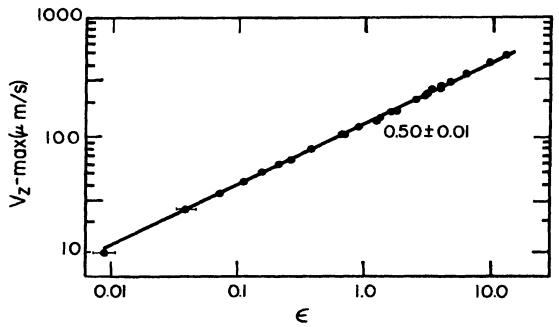

FIG. 8. The velocity v_z at one point in a convecting layer of oil vs $\varepsilon=(R-R_c)/R_c$, after Bergé (1975) [see also Bergé and Dubois (1974)]. On a log-log plot the slope is 0.50±0.01.

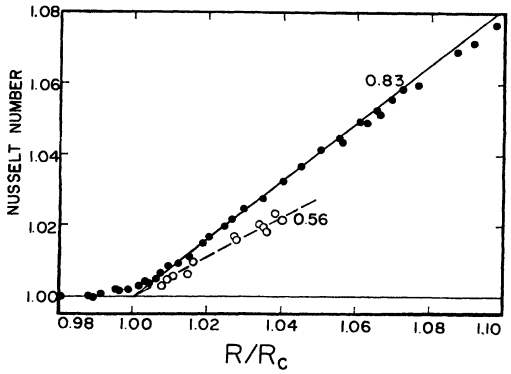

FIG. 9. Heat-transport data $N(R)$ vs R for two cylindrical containers having $\Gamma=4.72$ (solid symbols) and $\Gamma=2.08$ (open symbols), after Behringer and Ahlers (1977,1982).

Only the θ part of the temperature field appears in the average of (54), because the averaged product of the conductive portion of T and **v** vanishes. Since both v_z and θ grow as $\varepsilon^{-1/2}$ above R_c, $\langle Q_z \rangle$ should show a leading term proportional to ε. A convenient way of representing a heat-flux data consists of normalizing $\langle Q_z \rangle$ by the conductive portion, R. The resulting dimensionless quantity is called the Nusselt number, N:

$$N = 1 + \langle \theta v_z \rangle / R . \quad (55)$$

N is unity below R_c and should grow linearly in ε with slope S for $R > R_c$:

$$N = 1 + S\varepsilon + \cdots . \quad (56)$$

Experimental data by Behringer and Ahlers (1977,1982) which demonstrate this expectation are given in Fig. 9. These data pertain to measurements on liquid ^{4}He in cylindrical containers with $\Gamma=4.72$ and 2.08. Except for a very small region near R_c, N is well characterized by a linear term plus small higher-order corrections in ε. The rounding very near R_c is attributable to slight imperfections such as variations of the height d, or small thermal perturbations associated with the sidewalls. The pathology of imperfections has been treated by several authors, including Kelly and Pal (1976), Hall and Walton (1977), and Daniels (1977,1978). On balance, the $\varepsilon^{1/2}$ power law for the velocity and temperature perturbation is now well established.

D. Amplitude and phase equations

1. A simple example

Much of the rather complicated analysis contained in the expansion techniques of Schlüter, Lortz, and Busse (1965) can be represented in a simpler, more compact form, by an amplitude equation. Recent work has been done by Swift and Hohenberg (1977), Wesfreid *et al.* (1978), Cross (1980,1982), Cross *et al.* (1980,1983), Pomeau and Manneville (1981), Pomeau and Zaleski (1981), Ahlers *et al.* (1981), Greenside *et al.* (1982), and Greenside and Coughran (1983). Here, the idea originated

by Newell and Whitehead (1969) and Segel (1969), is that $\mathbf{v}$ and θ just above R_c will have a spatial dependence which strongly resembles the critical mode. The convective states just above R_c should be describable by simply giving the amplitude A corresponding to the projection of the motion onto this mode with, possibly, corrections for small adjustments in the shape of the rolls (Cross, 1980). Since A may depend on time, this approach has the added advantage of being able to describe in a simple way the growth and saturation of the steady-roll pattern. In addition, the effects of the sidewalls on the flow, which were not considered by Schlüter, Lortz, and Busse, can be understood using an amplitude equation within an analytical framework. This has been done recently by Cross (1982) and by Cross, Daniels, Hohenberg, and Siggia (1980,1983). These authors consider a number of different cases. Here it is useful to focus on one of the simplest possibilities in order to observe some of the pertinent features.

In the event that the fields $\mathbf{v}$ and θ depend, as in Fig. 1(a), only on z and one horizontal coordinate, chosen to be y, these quantities can be written in terms of an amplitude $A(y,t)$, which varies slowly in space by

$$\begin{aligned} v_y &= \varepsilon^{1/2}(Ae^{i\alpha_c y} - \text{c.c.})v_{y0}(z) + O(\varepsilon) , \\ v_x &= 0 , \\ v_z &= \varepsilon^{1/2}(Ae^{i\alpha_c y} + \text{c.c.})v_{z0}(z) + O(\varepsilon) , \\ \theta &= \varepsilon^{1/2}(Ae^{i\alpha_c y} + \text{c.c.})\theta_0(z) + O(\varepsilon) . \end{aligned} \tag{57}$$

If Eq. (57) is to be a valid solution to $O(\varepsilon)$, A must satisfy

$$\partial A/\partial t = \tau_0^{-1}(\varepsilon A - bA\,|\,A\,|^2 + \xi_0^2 \partial^2 A/\partial y^2) , \tag{58}$$

where τ_0 and ξ_0 are given by Eqs. (41) and (42). Several features of Eq. (58) are worth noting. (1) For early times, the growth of A from a small initial value is proportional to $e^{\varepsilon t/\tau_0}$. (2) The term $\partial^2 A/\partial y^2$ allows for an adjustment in the roll wave vector, an effect which is important near walls. (3) The cubic term in A will provide a saturation mechanism which limits the growth of A. This last property is particularly interesting. In the case that the term $\partial^2 A/\partial y^2$ is negligible, Eq. (58) becomes an ordinarily differential equation for $A(t)$. The solution for $R > R_c$ is

$$|\,A(t)\,|^2 = |\,A(\infty)\,|^2 e^{2t\varepsilon/\tau_0}/(C + e^{2t\varepsilon/\tau_0}) . \tag{59}$$

C is related to the initial value of A, and $A(\infty)$, the limiting value of A as $t \to \infty$, is

$$|\,A(\infty)\,| = (\varepsilon/b)^{1/2} . \tag{60}$$

Equation (60) reflects the fact that $\mathbf{v}$ and θ vary as $\varepsilon^{1/2}$ near R_c. The convective time

$$\tau_{RB} \equiv \tau_0/\varepsilon \tag{61}$$

clearly sets the final scale for the approach to steady convection, and experiments should show critical slowing down which is analogous to the behavior of a mean-field-like system near its critical point. This analogy can be pursued further by noting that $A \propto \varepsilon^{1/2}$ plays the role of an order parameter. Measurements of the critical slowing

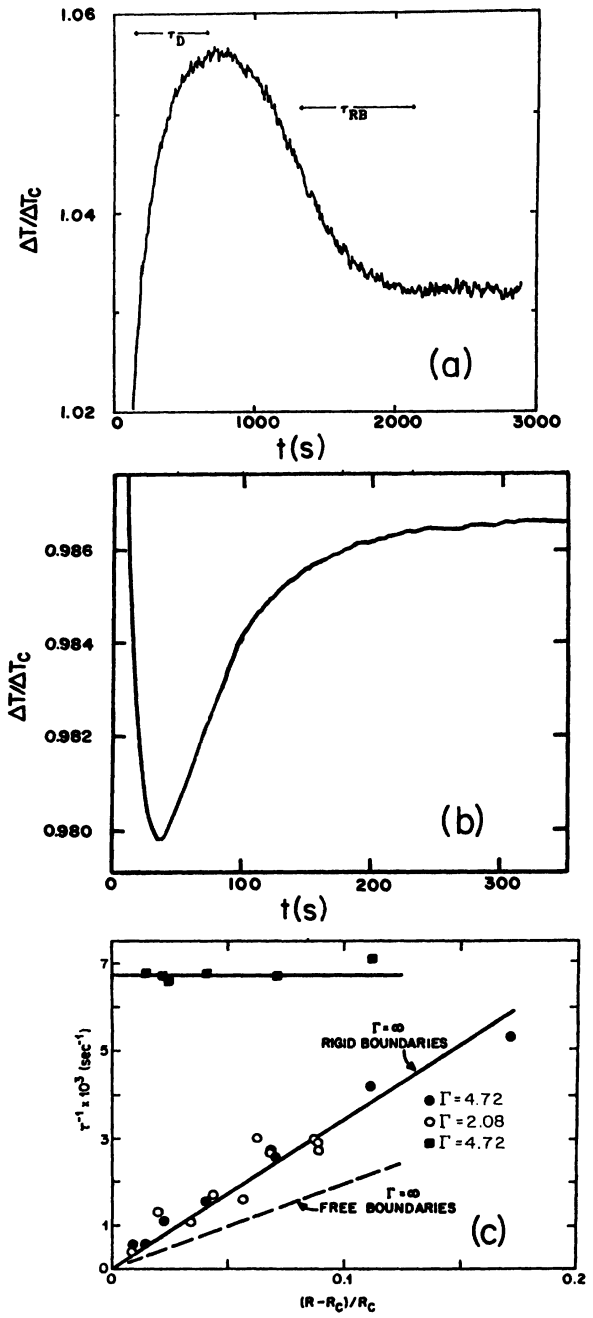

FIG. 10. (a) Final evolution of ΔT following a step increase in the heat current Q from below to above R_c. Data are for a $\Gamma = 4.72$ cylindrical container (Behringer and Ahlers, 1977). The section of the curve marked τ_D is dominated by the slowest diffusive thermal modes of Eqs. (31) and (32). The section marked τ_{RB} is dominated by the convective mode. (b) A similar time evolution for ΔT following a step decrease in Q from a steady convecting state to a subcritical state (Shaumeyer and Behringer, 1981) for a cylindrical container with $\Gamma = 6.22$. (c) Experimental data for the inverse of the observed convective relaxation time τ_{RB} vs ε, with the solid circles corresponding to $\Gamma = 4.72$, and the open circles corresponding to $\Gamma = 2.08$. The squares correspond to measurements of τ_D.

down were reported by Wesfreid *et al.* (1978) and by Behringer and Ahlers (1977) using liquid helium. In the latter experiments, the heat flux Q was increased instantaneously from a subcritical value to slightly supercritical value which remained fixed thereafter. The evolution of ΔT following such an event is shown some time after Q is switched on in Fig. 10(a). Initially, ΔT rises rapidly; then, as the diffusive modes of Eq. (31) decay, it moves toward a value which is higher than the long-time limit. Eventually, the slower convective modes begin to grow, causing the fluid to carry the heat more efficiently. The result is a decrease in ΔT as the system moves towards a steady state. During this final decay, ΔT should relax with a time constant of $\tau_{RB}/2$. The critical slowing down below R_c can be obtained by establishing a convecting state followed by a step decrease in Q to a subcritical value. An example of the ensuing relaxation is given in Fig. 10(b) for a cylindrical container with $\Gamma=6.22$ (Shaumeyer and Behringer, 1981). Analysis of the data for two different aspect ratios yielded the circles in Fig. 10(c), where the observed values of τ_{RB}^{-1} as well as the diffusive times τ_D, the longest of the relaxation times in Eq. (32), are given versus ε for the final state. The convective flows occurring in the $\Gamma=4.72$ container of Fig. 10(a) were later shown by Ahlers, Cross, Hohenberg, and Safran (1981) to have additional transient behavior requiring a more sophisticated analysis. However, the data give a semiquantitative demonstration of critical slowing down. The experimentally obtained data for τ_{RB}^{-1} are consistent with the linear dependence on ε of the slowest time scale. That the slope of the observed relaxation rates with respect to ε is found to agree with the $\Gamma=\infty$ value is justified through the calculations of Shaumeyer, Behringer, and Baierlein (1981) shown in Fig. 7(b), indicating that the growth rate of the critical mode is relatively insensitive to Γ until $\Gamma \lesssim 2$.

2. A Lyapunov functional and pattern formation

When one characterizes the steady states preceding turbulent onset, an important question involves determining the way in which the convection rolls adjust to the vertical walls and respond to initial transients. Unless particular care is taken, the rolls will not be uniformly aligned, and defects will form. Indeed, competition between boundary and bulk effects leads to textured and defected flow patterns. An amplitude equation, which under some conditions may be derived from a Lyapunov functional, is a useful tool that has been used recently by Cross (1982), Greenside *et al.* (1982), and Greenside and Coughran (1983) to address the problem of determining preferred flow patterns. A Lyapunov functional for a dynamical system, as discussed, for instance, by Hirsch and Smale (1974), has a lower bound and can only decrease or remain constant as the system evolves. Cross (1982) looks for solutions valid to $O(\varepsilon)$, allowing for roll curvature and having the form

$$\theta=\psi(x,y,t)\theta_0(z) , \tag{62}$$

$$v_x=u_0(z)(i\alpha_c)^{-1}\partial\psi/\partial x , \tag{63}$$

$$v_y=u_0(i\alpha_c)^{-1}\partial\psi/\partial y , \tag{64}$$

$$v_z=\psi v_{z0}(z) . \tag{65}$$

The equation of motion for ψ can be written in terms of the variation of a Lyapunov functional F given by

$$F=\int d^3r\{\tfrac{1}{2}\varepsilon^2-\tfrac{1}{2}\varepsilon\psi^2+\tfrac{1}{4}\bar{g}\psi^4 + \tfrac{1}{2}(\xi_0^2/4\alpha_c^2)[(\nabla^2+\alpha_c^2)\psi]^2\} , \tag{66}$$

where the term in ψ^4 is a representation of a kernel.

Then

$$\tau_0\dot{\psi}=-\delta F/\delta\psi . \tag{67}$$

The time derivative of F has the property

$$\dot{F}=-\tau_0\int d^3r(\partial\psi/\partial t)^2 , \tag{68}$$

i.e., it cannot increase in time. Hence the "preferred" state of the system has the smallest possible F. Cross (1982) has calculated F for various roll configurations. An important result of this analysis is the prediction that rolls will tend to intersect rigid nonslip walls in an approximately perpendicular direction. Gollub and Steinman (1981) and Gollub and Heutmaker (1984) have provided a particularly clear demonstration using laser Doppler velocimetry techniques on a large rectangular layer of convecting water. Results by Gollub and Heutmaker are shown in Fig. 11, which shows a computer-enhanced Doppler image of the flow in a large rectangle. Recently, a number of other experiments, including those by Croquette, Mory, and Schosseler (1983), Walden *et al.* (1983,1984), Steinberg, Ahlers, and Cannell (1984), and Croquette and Pocheau (1984), have used visualization techniques to study pattern formation.

The flow patterns in helium experiments have not yet proven accessible to direct observation, and two factors make visual observations very difficult. First, the dielectric constant of liquid helium is very nearly unity. Consequently even simple flow visualization through the

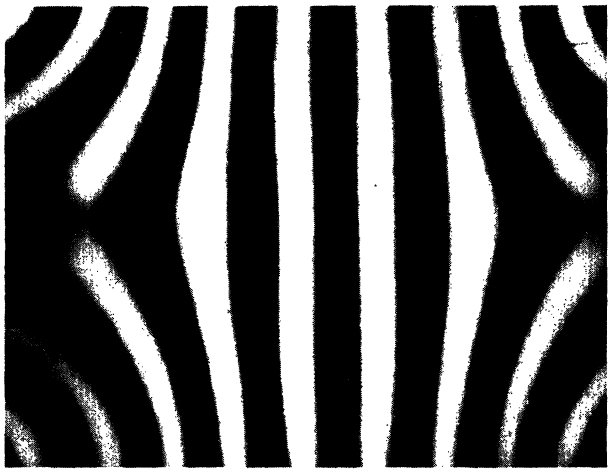

FIG. 11. A convective pattern observed using a Doppler velocimetry flow visualization technique with computer enhancement (Gollub and Heutmaker, 1984).

focusing-defocusing effects of induced gradients in the index of refraction is very difficult with helium. Second, the viscosity of helium is quite small, so that suspending small light-scattering objects in the fluid, a process complicated by electrostatic attraction of the particles to the walls, is also quite hard. In view of these difficulties, several alternative techniques for providing local information have been developed. For instance, Libchaber and Maurer (1978) have used very small thermal probes, and Ahlers and Behringer (1978b) have used ion currents as probes of the vertical velocity. These techniques have not been developed to the point of yielding information on the flow patterns.

Heat-transport data can be used, however, to infer possible roll patterns and other interesting information. Ahlers, Cross, Hohenberg, and Safran (1981) have fitted numerical integrations of amplitude equations to data showing the evolution of flow just above R_c. The data were obtained in a cylindrically confined helium layer having $\Gamma=4.72$, with experimental details to be found in Behringer and Ahlers (1982). A particularly interesting feature of the analysis by Ahlers *et al.* (1981) is their modeling of the mechanism responsible for the initial growth of A or ψ in Eqs. (58) or (67). Since these equations are homogeneous, they cannot describe instabilities growing from zero amplitude. An appropriate boundary or initial condition may be invoked to enforce a nonzero initial value, or an inhomogeneous forcing field may be added. Two possible sources for such a forcing field studied by Ahlers *et al.* (1981) are stochastic thermal noise and small perturbations which make the bifurcation to convection imperfect. Among the latter are imperfections in the cell geometry (Kelly and Pal, 1978), and heat flow injected from the side walls (Hall and Walton, 1977; Daniels, 1977,1978). Ahlers *et al.* (1981) showed that imperfections, as expressed as a constant inhomogeneous term, lead to a reasonable description of the onset of time dependence in data obtained following a step increase to a supercritical value of the heat current. However, a Langevin noise source, used to describe the effects of thermal noise, did not lead to a particularly good description of the initial system response to a heat current step. Figure 12 contrasts the two types of forcing functions by showing what the authors term a corrected heat flow versus time following the heat current step. As a consequence of this presentation, the data of Fig. 12 resemble an inverted form of Fig. 8(a), where the time evolution of ΔT is given following a step in Q. Using effectively a single-mode amplitude, and a fixed inhomogeneous term Ahlers *et al.* (1981) obtained the dashed line of Fig. 12(a). Experimental data are given by the solid circles. (The initial diffusive transients are not included in the model, only the convective transients.) The calculation for noise-initiated flow, again with effectively a single mode, is given by the solid line for Fig. 12(a), yielding a somewhat inferior description to the onset of convection. Here a noise amplitude 6×10^3 times bigger than that expected from statistical thermal noise is needed to provide an acceptable fit. The authors were able to provide good agreement with the data at later times by using more modes in the calculation as shown for Fig. 12(b) by the additional line. These authors also estimated the slope $S=dN/d\varepsilon$ for various flow patterns in a cylindrical container. In particular, they find $S=0.91$, 0.45, and 0.72 for concentric rolls with and without a central node and straight rolls, respectively. The experimentally obtained slope of $S=0.83$ (Fig. 9, $\Gamma=4.72$) is closest to the first of these possibilities, but additional work in this area would be valuable.

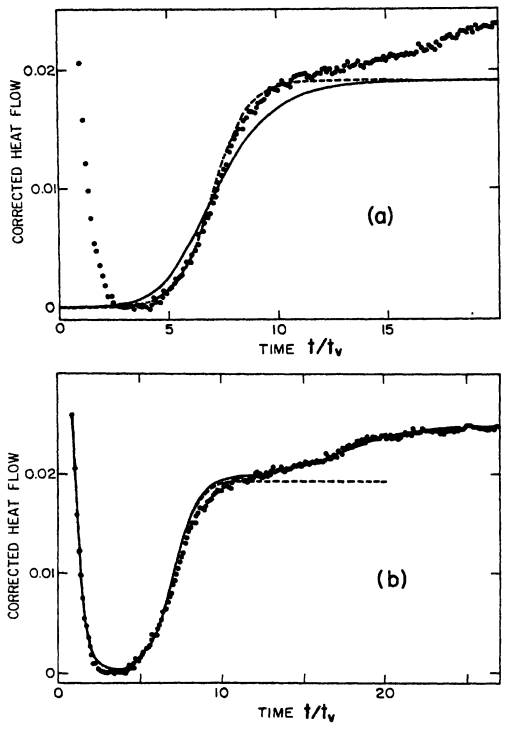

FIG. 12. Values of the "corrected heat flow" vs time following a step increase in the heat flux Q to the bottom of the layer, after Ahlers *et al.* (1981). (a) contrasts the experimental data (solid circles) with a fit (dashed line) to a deterministic model for the onset of convection containing only one amplitude and a fit (solid curve) to a model with one amplitude in which the onset of convection is initiated by a stochastic noise source. (b) The solid line shows a fit to a deterministic model where three amplitudes have been used. The dashed line reproduces the dashed line of (a).

E. Stability of convective rolls

The validity of the amplitude expansion is restricted to a region close to R_c, and for larger Rayleigh numbers steady solutions must be obtained by alternative techniques. The stability of these steady solutions plays an important role in the onset of turbulence. Using a Galerkin technique, Clever and Busse (1974), Busse and Clever (1979), and Bolton, Busse, and Clever (1983) have investigated the stability of steady parallel convective rolls in a

horizontally infinite layer to infinitesimal disturbances. It is anticipated that these calculations should apply to large Γ experiments. The wave number α of the rolls influences their stability, as shown by Fig. 13, which gives the stability diagram (Busse and Clever, 1979) for Pr=0.71, a value typical for helium. The convective stability boundary, after Fig. 6, is indicated by the dashed line; additional instabilities also occur, as indicated. Within the shaded region straight parallel rolls are expected to be linearly stable. For other Prandtl numbers the details of the stability diagram may change, but generally there is an enclosed region in which straight parallel rolls are found to be the only linearly stable solutions for a horizontally infinite Boussinesq layer. In this regard, for helium the most important boundaries are the skewed varicose instability and the oscillatory instability, since the rolls must undergo a transition at these boundaries as R increases. When the Rayleigh number increases across the oscillatory instability boundary which can occur if α is small, the rolls undergo coherent periodic oscillations as sketched in Fig. 14(a). For larger wave vectors the skewed varicose instability is important. When the Rayleigh number crosses this boundary, the rolls acquire a superimposed structure as sketched in Fig. 14(b); the choice of name is clearly appropriate. Unlike the oscillatory instability, the skewed varicose instability is expected to occur at onset without time dependence. The importance of these instabilities to the onset of turbulence is included in the discussion following. If the Rayleigh number is decreased from an initial value lying inside the shaded region, the system will encounter either the Eckhaus instability (Eckhaus, 1965; Stuart and DiPrima, 1978) or the zigzag instability (Busse, 1981). The first of these is an instability which forms parallel to the original rolls, and the second is a steady sinusoidal perturbation which is observed experimentally at angles of 40° and 140° relative to the original rolls.

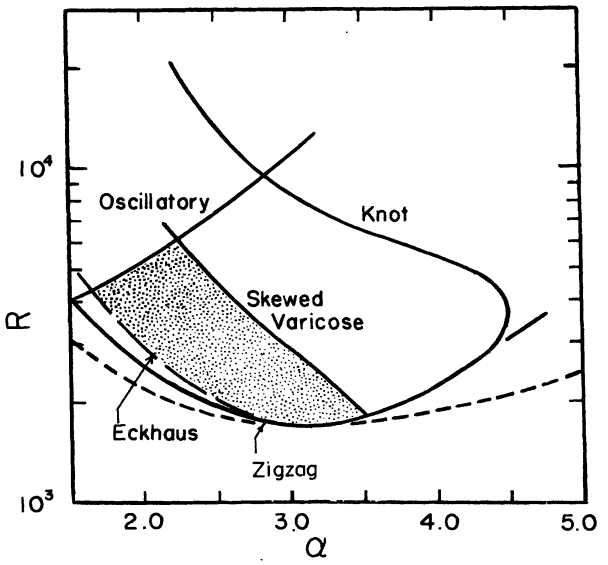

FIG. 13. Stability boundaries R vs α for a fluid of Pr=0.71, after Busse and Clever (1979). Straight parallel rolls are expected to be stable within the shaded region. The dashed line gives the neutral stability curve for the onset of convection. The boundaries for various instabilities on straight rolls are indicated.

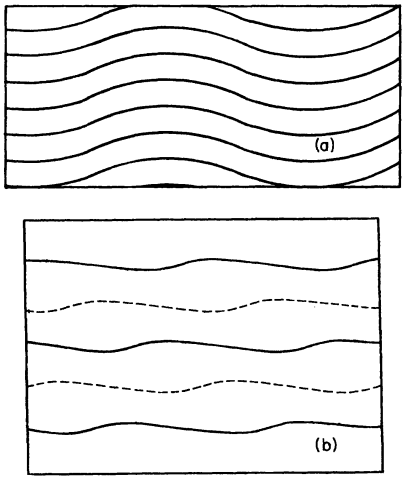

FIG. 14. Schematics of important instabilities for straight parallel convective rolls. (a) The oscillatory instability. In this case there will be a superposed structure on the straight rolls which oscillates coherently with the wavy structure shown. (b) The skewed varicose instability. In this case the superposed pattern, as sketched, is expected to be time independent. See Busse and Clever (1979).

IV. TURBULENCE

A. Introduction

One of the most intriguing phenomena occurring in fluids is turbulence. Although strongly turbulent flows have been studied in the past, much recent work has focused on the evolution of turbulence. An important advance involves the application of mathematical theories of dynamical systems to turbulent onset in physical systems such as a convecting fluid. Here, the discovery of strange attractors plays a particularly significant role. A number of reviews describe recent theoretical developments, including those by Eckmann (1981), Ott (1981), Yorke and Yorke (1981), the conference proceedings introduced by Swinney (1983), and the report by Abraham, Gollub, and Swinney (1984). Accordingly only a brief summary is given beginning in Sec. IV C.

Reformulating the equations of motion is useful for making formal contact with this work. Near the onset of time dependence the basic roll patterns are expected to coexist with a superposed time-dependent flow. This concept is expressed by looking for solutions of Eqs. (45) and (46) of the form

$$\bar{u}=\bar{u}_0(\mathbf{r})+\Delta\bar{u}(\mathbf{r},t)\ , \tag{69}$$

where $\bar{u}_0(\mathbf{r})$, which has a solenoidal velocity part, corresponds to a steady solution such as straight rolls, and $\Delta\bar{u}$ is a finite perturbation. Equation (45) becomes, with Eq. (69),

$$[\partial\Delta\bar{u}/\partial t+(\bar{u}_0\cdot\bar{\partial})\Delta\bar{u}+(\Delta\bar{u}\cdot\partial)\bar{u}_0-\mathbf{H}\Delta\bar{u}+\bar{\partial}\Delta w]+(\Delta\bar{u}\cdot\bar{\partial})\Delta\bar{u}=\mathbf{H}\bar{u}_0-(\bar{u}_0\cdot\bar{\partial})\bar{u}_0-\bar{\partial}w_0 \ . \tag{70}$$

The terms have been segregated to emphasize the linear and nonlinear parts in the perturbation as well as the steady solution. The right side of Eq. (70) vanishes by assumption. The linearized problem, contained in the bracketed terms of (70) can be written in the form

$$\partial\Delta\bar{u}/\partial t=\mathbf{H}\Delta\bar{u}-\partial\Delta w \ , \tag{71}$$

where $\mathbf{H}$ is a linear matrix operator depending on $\bar{u}_0$, R, and P. The linear terms proportional to $\bar{u}_0$ and contained in $\mathbf{H}$ are inherently non-Hermitian for nonzero $\bar{u}_0$. If solutions to (71) are sought which have the form

$$\bar{u}(\mathbf{r},t)=e^{\sigma t}\bar{U}(\mathbf{r}) \ ,$$

the presence of non-Hermitian terms in $\mathbf{H}$ for $R>R_c$ allows the possibility of complex values of σ and hence oscillatory motion as in the oscillatory instability predicted by Clever and Busse (1974).

The effect of the nonlinear term $(\Delta\bar{u}\cdot\bar{\partial})\Delta\bar{u}$ can be reexpressed by expanding $\Delta\bar{u}$ in a complete set of functions $\{\bar{u}_i(\mathbf{r})\}$ with time-dependent amplitudes:

$$\Delta\bar{u}(\mathbf{r},t)=\sum_i c_i(t)\bar{u}_i(\mathbf{r}) \ . \tag{72}$$

The functions $\{\bar{u}_i(\mathbf{r})\}$ must satisfy the appropriate boundary conditions, and $\bar{\partial}\cdot\bar{u}_i=0$. One possible choice for the expansion functions, assuming completeness, is the set $\{\bar{S}_i\}$ satisfying

$$\sigma_i\bar{S}_i=\mathbf{H}\bar{S}_i-\bar{\partial}w_i \tag{73}$$

and appropriate boundary conditions. A formal solution for the time-dependent amplitudes $\{c_1(t)\}$ is obtained by using Eq. (72) in Eq. (70), and by taking appropriate scalar products to project out each time derivative $c_i(t)$. Since $\mathbf{H}$ is non-Hermitian, the members of the set $\{\bar{S}_i\}$ are not mutually orthogonal and a set of functions $\{\bar{S}_i^{+}\}$ satisfying the Hermitian conjugate problem must be constructed. The conjugate modes are orthogonal to the modes of the original problem and yield the equations

$$\dot{c}_i=\sigma_i c_i+\sum_{jk}M_{ijk}c_jc_k \ , \tag{74}$$

with

$$M_{ijk}=-\langle\bar{S}_i^{+},(\bar{S}_j\cdot\bar{\partial})\bar{S}_k\rangle=+\langle(\bar{S}_j^{*}\cdot\partial)\bar{S}_i^{+},\bar{S}_k\rangle \ . \tag{75}$$

The infinite set of Eq. (74) provides a formal description of the problem. In practice, no calculations have been done which could accurately describe an experiment. Instead experiments have usually been compared with tractable models, generally having only a few amplitudes, in anticipation, partly justified, that turbulence in nonlinear systems will evolve in only a fairly small number of ways. This approach, discussed in the following section, applies to a broad spectrum of systems including convective flows. However, McLaughlin and Martin (1974,1975) have performed computations on a set of coupled equations with a large number of modes and a Prandtl number $\mathrm{Pr}=1$, appropriate to liquid helium. On integrating the equations of motion, they found a number of interesting time-dependent states which resemble some of those observed experimentally. More importantly, this work was seminal, because it attempted to demonstrate the possibility of strange attractors as a cause for the onset of turbulence.

Before we abandon a formally exact description, Eq. (74) provides additional information about the possibility of turbulence near R_c. For $R<R_c$ the quantity r defined by

$$r=\sum_i |c_i|^2 \tag{76}$$

is a Lyapunov functional for the problem. This follows [see also Joseph (1976)] by considering dr/dt. By inspection of (75), $M_{ijk}=-M_{kji}$ for $R<R_c$, because there $\bar{S}_i^{+}=\bar{S}_i=\bar{S}_i^{*}$. The mode amplitudes c_i are also real, so that as a consequence of Eq. (74),

$$dr/dt=2\sum_i\sigma_i c_i^2 \ , \tag{77}$$

which is negative for the conduction-only solution when $R<R_c$. Accordingly, below R_c, the conductive solution always evolves as $t\to\infty$, regardless of the initial conditions. Above R_c

$$dr/dt=2\,\mathrm{Re}\left\{\sum_i\sigma_i|c_i|^2+\sum_{ijk}M_{ijk}c_i^{*}c_jc_k\right\} \ . \tag{78}$$

The terms in Eq. (78) which involve $\{M_{ijk}\}$ vanish at R_c at least as fast as ε. Consequently, Eq. (78) leads to the expectation that for some range of positive but small enough ε steady flows will evolve for reasonable initial conditions as long as the roll pattern corresponding to $\bar{u}_0$ is initially stable, i.e., $\mathrm{Re}(\sigma_i)<0$ for all i.

B. When is turbulence present?

A discussion of turbulence should begin with a prescription for recognizing when turbulence is present. On this point, there often exists a dichotomy in theoretical and experimental approaches. A theoretical description of a system may involve a rule for generating a sequence of points or it may involve a set of nonlinearity coupled ordinary differential equations in some set of variables $\{c_i(t)\}$, $i=1,\ldots,n$ (Guckenheimer and Holmes, 1983). Equation (74) is a particular example. Members of the set $\{c_i\}$ form a phase space, and the equations of motion, with initial conditions, describe trajectories in the phase space. If all trajectories originating from some set in phase space converge toward a common subset of phase space, the subset is called an attractor, and the set of all initial states leading to the attractor is the basin of attraction. Turbulence occurs if the trajec-

tories are nonperiodic and have correlation functions for dynamical quantities $x(t)$

$$\lim_{t\to\infty} t^{-1}\int_0^t [x(t)-\langle x\rangle][x(t+\tau)-\langle x\rangle]$$

which vanish as $\tau\to\infty$ and a sensitive dependence on initial conditions (Ott, 1981).

The experimental determination of turbulence is often less well defined, principally because the amount of information is small and observations times are finite. Usually one quantity is measured which is related to a superposition of the variables $\{c_i\}$. For instance, the vertical velocity $v_z(\mathbf{r}_0,t)$ at a position $\mathbf{r}_0$ within the fluid may be measured. In helium experiments temperature fluctuations, effectively averaged over the bottom of the layer are frequently measured. These correspond via Eqs. (69) and (74) to

$$\delta T(t)=\sum_i c_i(t)\int \Delta\theta_i(\mathbf{r})dx\,dy\ . \tag{79}$$

A useful tool is the experimental power spectrum [see, for instance, Otnes and Enochson (1972)] defined for a quantity such as $\delta T(t)$ which is measured over a time interval τ:

$$P(\omega)=\tau^{-1}\left|\int_0^\tau \delta T(t)e^{i\omega t}dt\right|^2 . \tag{80}$$

The integrals are done on a discrete set of data points via a fast Fourier transform, and appropriate windowing must be done to suppress side lobes spuriously generated by the finite measurement time. If the resulting power spectrum contains features which are broader than the instrumental frequency resolution of order τ^{-1}, then the expectation is that the flow is turbulent. Inherent in this method are the possibilities that the observation times are too short, the sampling rate too slow, or the experiments obscured (possibly altered) by the presence of external noise.

A new technique for identifying turbulence involves calculating the dimension of an attractor from experimental time series. In this procedure (Packard, Crutchfield, Farmer, and Shaw, 1980), an orbit in a phase space of arbitrarily high dimension n is created by converting a series of data $x_1,x_2,\ldots,x_n,\ldots$, taken at uniform time intervals Δt to a time series of n-tuplets $(x_i,\ x_{i+k},\ x_{i+2k},\ldots,x_{i+(n-1)k})$. As long as n is sufficiently large and the experimental error sufficiently small, the resulting phase-space orbit is equivalent to one which would be generated in a more conventional set of phase-space coordinates, such as those of Eq. (74). Given a phase-space description of the orbit, a number of powerful analytical tools (Grassberger and Procaccia, 1983a,1983b; Farmer, Ott, and Yorke, 1983; Roux, Simoyi, and Swinney, 1983) are available for calculating its dimension, a quantity which can be defined in a number of ways, but which is expected to be nonintegral when turbulence due to a strange attractor is present.

C. Pictures of the onset of turbulence

1. Introduction via the Landau-Hopf model

One of the most important contributions of dynamical systems theory is the demonstration that turbulence can occur in systems with only a few degrees of freedom. This section reviews the Ruelle-Takens-Newhouse picture and generally recognized scenarios for the onset of turbulence; the following section gives examples from the helium literature. The classical description of the origins of turbulence, due to Landau (Landau and Lifshitz, 1959) and Hopf (1948), requires an arbitrarily large number of degrees of freedom. In this model, the expectation is that as the Rayleigh number increases, there will be a series of bifurcations to oscillatory modes. The nonlinear coupling between the modes is assumed to have no other result than the generation of a set of sum and difference frequencies formed from the fundamental frequencies of the oscillatory modes. An experimental observation on such a system would reveal a power spectrum with isolated, instrumentally sharp peaks. Consequently, there is no well-defined onset of turbulence in this model; rather, an experimenter would conclude that the flow was turbulent when his apparatus could no longer resolve the individual peaks.

Although the Landau picture is generally not correct, bifurcations to periodic or multiply periodic states do occur. The simplest periodic flows can occur in systems described by two degrees of freedom, and the periodic attractors are closed curves. When three or more degrees of freedom exist, multiply periodic attractors and strange attractors are added to the possible occurrences. Multiply periodic orbits are characterized by two or more incommensurate frequencies; their attractors are tori. A strange attractor is a very complex region of phase space, now commonly associated with the onset of turbulence.

2. The Ruelle-Takens-Newhouse picture

A useful guide in understanding the onset of turbulence has been provided by Ruelle and Takens (1971) and Newhouse, Ruelle, and Takens (1978). Their results refer to general systems characterized by some parameter which for convective flows corresponds to R. As R increases, the system undergoes a series of bifurcations to oscillatory states. Ruelle and co-workers have argued that as a generic property, nonlinear systems should have a strange attractor after the third bifurcation. Recently, Grebogi, Ott, and Yorke (1983) have shown the Ruelle-Takens-Newhouse picture does not apply in all cases, particularly if the nonlinear effects are weak. This helps explain several experimental counterexamples to the scenario put forward by Walden, Kolodner, Passner, and Surko (1984), Gollub and Benson (1980), and Libchaber, Fauve, and LaRoche (1983). In the example of Walden *et al.* up to five independent frequencies occurred at one time. However, the motion associated with each frequency was spa-

tially localized; possibly the interaction between the various types of motion was weak. In the remaining examples, three distinct frequencies were observed without the occurrence of turbulence. However, as discussed below and by Swinney (1983), a number of investigations into the onset of convective turbulence have revealed behavior which resembles the expectations suggested by Ruelle, Takens, and Newhouse.

3. The Lorenz model

Strange attractors arise in a number of mathematical systems which have been extensively studied and which provide a conceptual springboard for understanding the onset of turbulence in experiments. The earliest mathematical model of turbulence with a strange attractor was studied by Lorenz (1963), with more recent work on the model discussed by Guckenheimer and Williams (1976), Kaplan and Yorke (1979), Manneville and Pomeau (1979,1980), and Yorke and Yorke (1981). It has also been used (Ahlers, Hohenberg, and Lucke, 1984,1985) as a tool for understanding the response of a convecting layer to a modulation in the heat current. In this case the experiments were carried out on a liquid-helium layer.

The model consists of three coupled equations which were originated by Saltzman (1962) as a very abbreviated description of convection; in fact, these equations are more appropriate to a convection loop (Welander, 1967; Gorman, Widmann, and Robbins, 1984). The equations, having adjustable constants r, Pr, and b, are

$$\begin{aligned} \dot{c}_1 &= -\mathrm{Pr}(c_1 - c_2) , \\ \dot{c}_2 &= -c_2 + r c_1 - c_1 c_3 , \\ \dot{c}_3 &= c_1 c_2 - b c_3 . \end{aligned} \tag{81}$$

The parameter r is equivalent to R/R_c, and the parameter b is related (McLaughlin and Martin, 1975) to the roll wave vector. Stable convective flows begin when r exceeds 1; for $0 < r < 1$ the stable solution is conductive and corresponds to $c_1 = c_2 = c_3 = 0$. When $1 < r \lesssim 24$ (with the usual choice $b = \frac{8}{3}$, $\sigma = 10$), there are two stable solutions corresponding to two convective flows which differ in the sense of the roll stream lines (see Fig. 1). These steady solutions occur at $c_1 = c_2 = \pm[b(r-1)]^{1/2}$, $c_3 = r - 1$, as indicated by the points in Fig. 15. Above $r = 24.06$ but below $r = 24.74$ several different orbits can occur depending on the initial conditions. When r exceeds 24.74, the orbits are chaotic. The motion encircles the formerly stable steady solutions with the number of loops near a given point before encircling the other, a highly sensitive function of the initial data. An example of such a chaotic orbit, projected onto the $c_3 - c_2$ plane, appears in Fig. 15. As r is raised further, additional features arise including regimes of periodic as well as turbulent flows (Manneville and Pomeau, 1980).

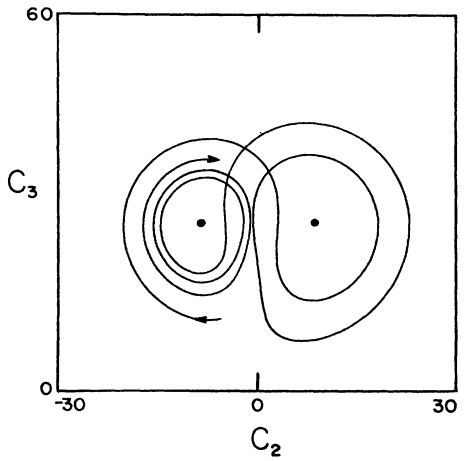

FIG. 15. Projection onto the $c_3 - c_2$ plane of an orbit for the Lorenz model, with $r = 28$, $\mathrm{Pr} = 10$, and $b = \frac{8}{3}$. The dots are unstable fixed points; below $r = 24.74$ these become stable.

4. One-dimensional noninvertible maps

An important theoretical development has come from noninvertible one-dimensional iterative maps. These maps generate a sequence of points which can be regarded as a time series, and related to three-dimensional ordinary differential equations as discussed by Ott (1981). An extensively studied map, the logistic model, considered by May (1976) and Feigenbaum (1978,1979) generates a sequence of points lying in the interval (0,1) by

$$x_{n+1} = 4b x_n (1 - x_n) \tag{82}$$

so long as $0 < b < 1$. As b increases, a series of bifurcations occurs. The first bifurcation at $b = \frac{1}{4}$ changes the stable state of the system from $x = 0$ to another point $x^* = 1 - (4b)^{-1}$. The next bifurcation occurs to a periodic state of alternating points $x_1, x_2, x_1, \ldots$, and successive bifurcations occur to periodic states of successively doubled length. An accumulation point occurs for $b = 0.862\ldots$, and the b_k, the bifurcation values of b to 2^k point cycles, satisfy

$$\lim_{k \to \infty} \frac{b_k - b_{k-1}}{b_{k+1} - b_k} = 4.699\ldots . \tag{83}$$

As each subharmonic bifurcation occurs, the power at the new frequency is expected to be reduced by a constant factor from the previous one. Above the accumulation point various regimes of periodic behavior are interspersed with noisy behavior. A particularly important result has been obtained by Feigenbaum (1978,1979) showing that the period doubling properties of Eq. (82) are universal, depending only on the qualitative shape of the map, and not on its details.

5. Intermittency

One additional description of the onset of turbulence is due to Manneville and Pomeau (1979,1980). In a strict sense, this scenario applies when a stable periodic attrac-

tor and an unstable attractor merge; in convective flows this occurs as the Rayleigh number increases toward $R = R_t$. Above R_t sections of a seemingly laminar periodic flow lasting for times $\sim(R - R_t)^{-1/2}$ are interrupted by episodes of noisy behavior. The term *intermittency* is sometimes applied loosely to flows characterized by regimes of periodic or steady behavior interspersed with nonperiodic interludes.

D. Experimental observations of turbulence

1. Evolution of turbulence in small layers

Experiments on convecting layers typically show behavior which resembles the previously discussed theories when the aspect ratio Γ is small. The reason for this is fairly clear; when the aspect ratio is small, only a small number of modes should be relevant, the rest being heavily damped. An example drawn from the helium literature demonstrates an onset to turbulence after a doubly periodic regime. Figure 16 shows power spectra obtained by Ahlers and Behringer (1978a,1978b) using a cylindrical container with $\Gamma = 2.08$. The spectra were calculated from temperature fluctuations with fixed applied heat flux. Here fluctuations δT in the total temperature difference ΔT are expressed in a dimensionless form $\delta T/\Delta T_c$. At the beginning of the sequence two frequencies and their harmonic combinations are present. Over a short span of Rayleigh numbers, the flow is characterized by a broad-band spectrum. Other results have been obtained by Gollub and Benson (1980) using a low—aspect-ratio rectangular layer of water. Their results show several different routes to turbulence, which fall within the types of behavior seen in nonlinear systems with a few degrees of freedom.

Examples demonstrating an onset to turbulence via period doubling are available from several studies of convection; in particular, these include work by Libchaber and Maurer (1980), Gollub, Benson, and Steinman (1980), and Libchaber (1983). Figure 17 focuses on the liquid-helium measurements of Libchaber and Maurer (1980). [See also Libchaber (1983).] In this sequence of power

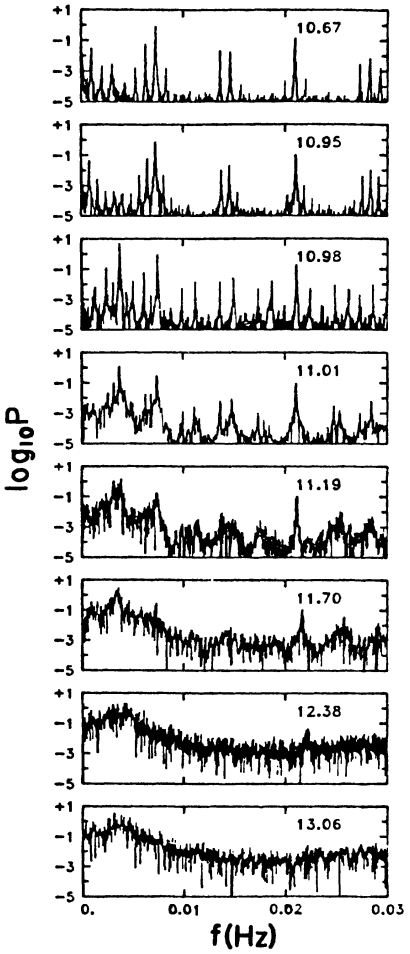

FIG. 16. The onset of turbulence in a small aspect-ratio cylindrical layer of liquid helium, $\Gamma = 2.08$, after Ahlers and Behringer (1978a,1978b). Each figure gives the measured power P vs frequency f for temperature fluctuations $\delta T/\Delta T_c$ for a different value of R/R_c, as indicated by the number in the upper right-hand corner. The spectrum for $R/R_c = 10.67$ consists of instrumentally sharp peaks at two frequencies and their combinations. Over a fairly narrow range in R/R_c the peaks broaden and for the most part disappear into a continuous spectrum.

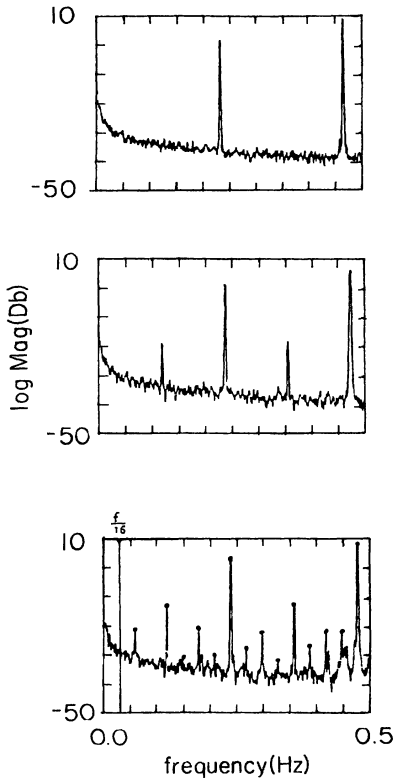

FIG. 17. Amplitude (power) vs frequency for temperature fluctuations showing the onset of turbulence via period doubling in a layer of liquid helium, after Libchaber and Maurer (1980) and Libchaber (1983).

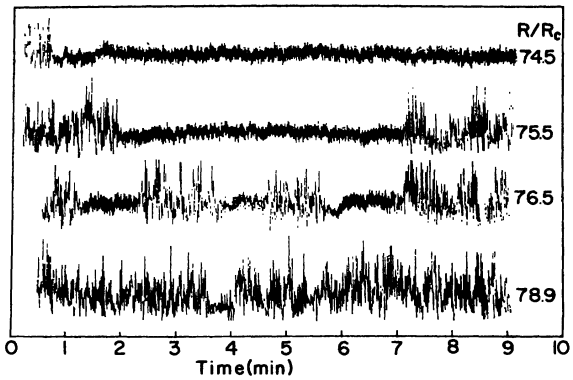

FIG. 18. The onset of turbulence via intermittent noise bursts which disrupt otherwise doubly period flows (Maurer and Libchaber, 1980).

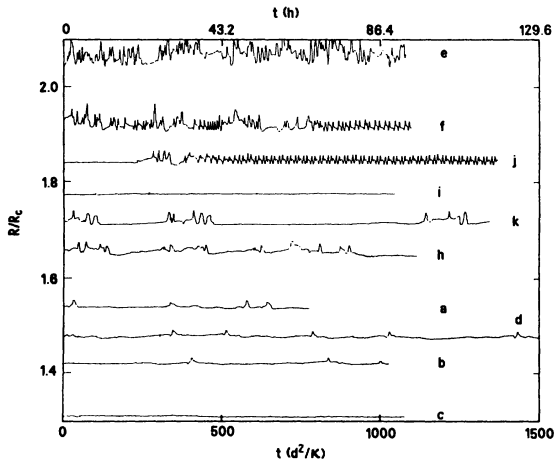

FIG. 19. The onset of turbulence for a moderate-size layer of liquid helium, $\Gamma=4.72$, after Ahlers and Walden (1980). These data, obtained at a series of fixed heat currents, show fluctuations in ΔT scaled by ΔT_c, hence in R/R_c, over extended observation times. The vertical scale indicates the relative size of the fluctuations and the time-average value of R/R_c.

spectra for local temperature fluctuations several period-doubling bifurcations occur. A complete cascade is not seen because of the effect of external perturbations. The spacing in R is in agreement with the prediction of Eq. (83). Likewise, the multiplicative decrease in the power of each new subharmonic frequency is seen.

The onset to turbulence via intermittency has been observed in seminal experiments by Maurer and Libchaber (1980) using a liquid-helium layer in a rectangular container with dimensions $2.3d\times1.2d\times d$, as in the experiments described above [see also Dubois, Rubico, and Bergé (1983)]. Their results are shown in Fig. 18. For the lowest Rayleigh number shown, $R/R_c=74.5$, the signal is a doubly periodic state consisting of two frequencies $f_1\simeq1.0$ Hz and $f_2\simeq0.3$ Hz with their combination frequencies. With increasing R/R_c the intermittent bursts of noise, only marginally present for $R/R_c=74.5$, become increasingly dominant. However, Maurer and Libchaber (1980) report that the regions of laminar (steady periodic) flow vary as $(R-R_t)^{-\beta}$, with $1<\beta<1.5$, although $\beta=\frac{1}{2}$ is expected theoretically (Manneville and Pomeau, 1979,1980).

2. Evolution of turbulence in large layers

If the aspect ratio is sufficiently large, a considerable number of modes may be relevant, and the relatively simple scenarios of turbulent onset given in Sec. IV.C may fail to describe experiments. That the aspect ratio significantly affects the evolution of turbulence was demonstrated by liquid-helium measurements. Some examples of the effects of aspect ratio are given in Figs. 19–21. These show temperature fluctuations for cylindrical containers with aspect ratios 4.72 and 6.22, obtained by Ahlers and Walden (1980) and Behringer, Shaumeyer, Clark, and Agosta (1982), respectively [see also Walden (1983)]. Each curve was obtained for fixed heat flux corresponding to the indicated time-averaged reduced Rayleigh number, R/R_c, and fixed top temperature. Even though the two aspect ratios differ by relatively little, the preturbulent flows are quite dissimilar. Other thermal measurements by Ahlers and Behringer (1978a,1978b) indicate that turbulence may occur quite soon after the onset of

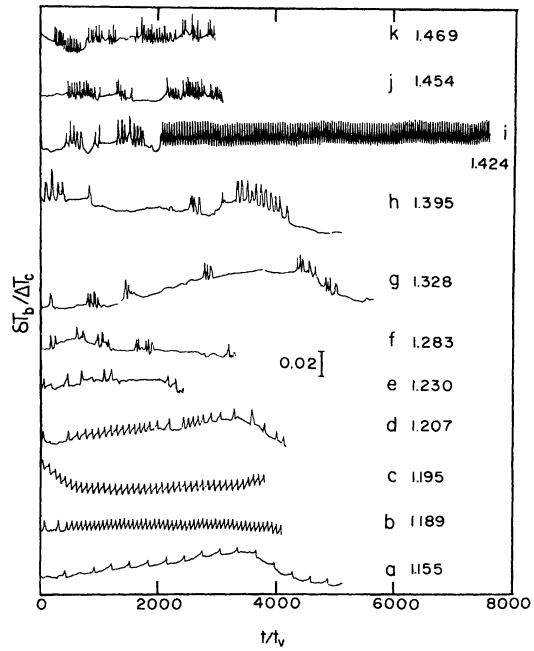

FIG. 20. The onset of turbulence for a somewhat larger cylindrical layer of fluid, $\Gamma=6.22$, after Behringer *et al.* (1982), showing fluctuations in the temperature at the bottom of the layer δT_b vs t/t_v at fixed Q and top temperature. These results, which are continued in Fig. 21 should be compared to Fig. 19 obtained with the same experimental conditions but different aspect ratio. The vertical bar indicates variations in $\delta T/\Delta T_c$ of 0.02 and the numbers give the time-average value of R/R_c.

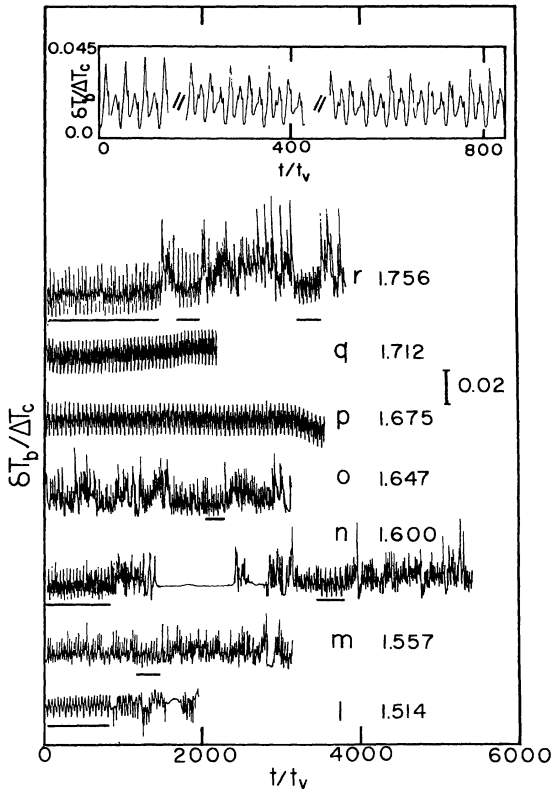

FIG. 21. A continuation of Fig. 20 showing the onset of turbulence for a cylindrical layer of liquid helium with $\Gamma=6.22$. Persistent turbulence was found for values of $R/R_c > 1.756$ after the regime of period multiplication shown in the inset.

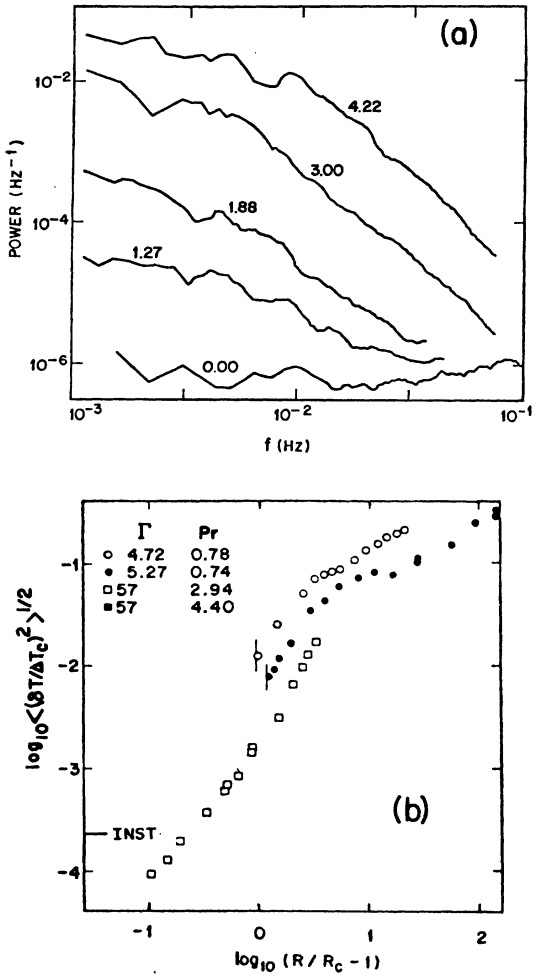

FIG. 22. (a) Power spectra for temperature fluctuations $\delta T/\Delta T_c$ at the indicated values of R/R_c for a $\Gamma=57$ cylindrical layer. These data (Ahlers and Behringer, 1978a,1978b) show the broad-band noise present close to the onset of convection. The instrumental noise level is given by the spectrum marked 0.0. (b) The rms values of $\delta T/\Delta T_c$, equivalent to the integrated power vs $R/R_c-1=\varepsilon$, for the aspect ratios and Prandtl numbers indicated. The instrumental noise is indicated by a horizontal bar next to the label INST.

convection for very large aspect-ratio layers. For $\Gamma=57$, Ahlers and Behringer found an onset to broad-band time dependence, as shown in the power spectra of Fig. 22(a), which exceeded the background noise level when $R/R_c \gtrsim 1.1$. Root-mean-square values of $\delta T/\Delta T_c$ for this aspect ratio, equivalent to the integrated power, are shown in Fig. 22(b) and compared with results for other aspect ratios. The onset of convection and the onset of time dependence are not well distinguished in this case, which is a surprising result in view of Sec. IV.A. Cross and Newell (1984) have developed a phase theory (Pomeau and Manneville, 1981) to describe gradual changes in the roll orientations in imperfect patterns; this work suggests that the broad-band noise is caused by pattern adjustments occurring over a time scale large compared to the horizontal diffusion time $t_H=\Gamma^2 t_v$, with the fluid eventually approaching a steady state. Additional experimental tests are clearly in order.

Recent measurements by Gao and Behringer (1984) and Behringer, Gao, and Shaumeyer (1983) provide a unified picture of the effects of aspect ratio on the onset of time dependence and raise some additional questions. Thermal measurements were obtained using liquid ^{4}He and an apparatus with cylindrical geometry that allowed a continuous variation of the aspect ratio over the range $2.4 \lesssim \Gamma \lesssim 22$. These measurements show that over the complete range of Γ there is a well-defined transition occurring at a Rayleigh number $R_1 > R_c$ associated with the onset of time dependence. Figure 23 gives values of R_1/R_c as a function of Γ. One notable feature is the tendency of the data to fall on a succession of sloping lines; in addition, for large Γ, $R_1/R_c \to 1.09$. Although there exists a well-defined transition, for all aspect ratios its qualitative nature changes. When Γ is small, $\Gamma \lesssim 4$, the transition occurs as a change in flow pattern, as manifested in Nusselt-number data; at the transition $N(R)$ shows a discontinuity as shown in the inset of Fig. 23. Additional transitions occur with increasing Rayleigh number for these small aspect ratios, and these are indicated by arrows at the transition points R_2 and R_3 in the example of the inset of Fig. 23. The Nusselt curve terminates at

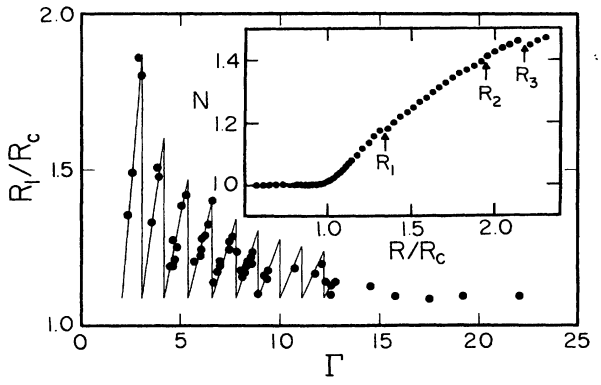

FIG. 23. Values of R_1/R_c vs Γ for cylindrical containers, after Gao and Behringer (1984). Here R_1 gives the Rayleigh number of the first instability above the onset of convection. The inset shows Nusselt number (heat transport) data for a small aspect-ratio ($\Gamma=3.253$) cylindrical container. Changes in the flow pattern occur at R_1, R_2, and R_3.

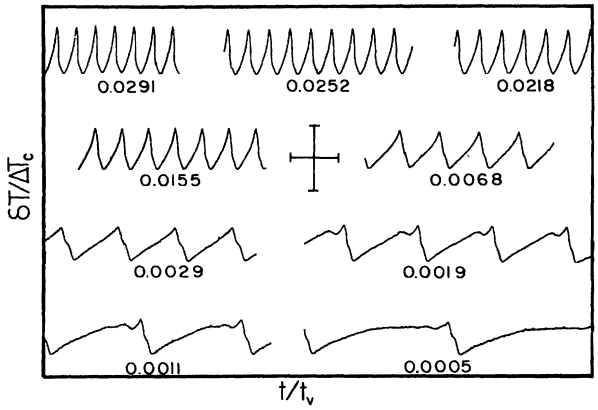

FIG. 24. A set of experimental data for $\delta T/\Delta T_c$ vs t/t_v showing the slowing down of a "Type II" periodic flow as $\varepsilon_1=(Q-Q_1)/Q_1$ approaches zero from above. The numbers under each curve indicate the values of ε_1. The data pertain to a $\Gamma=9.002$ cylindrical layer (Behringer, Gao, and Shaumeyer, 1983).

the onset of persistent time dependence, a point which is often associated with a flow pattern change and non-periodic flow. As Γ is increased, the transition changes character. Instead of a pattern change, R_1 corresponds to the onset of periodic flow, as long as $\Gamma \gtrsim 4$.

For $\Gamma \gtrsim 4$ and $R \gtrsim R_1$, periodic states occur which have an interesting but unexpected structure not attributable to the oscillatory instability. Indeed, the values of R_1 are too small to correspond to this instability which in liquid-helium measurements has been observed only after the onset of turbulent flow (Ahlers and Behringer, 1978b). For moderate aspect ratios, $4 \lesssim \Gamma \lesssim 13$, the most frequently observed behavior near R_1 is finite amplitude oscillations characterized by a frequency which vanishes as $\varepsilon_1^{1/2}$ as $R \to R_1^+$. Here ε_1 is defined by $\varepsilon_1 \equiv (Q-Q_1)/Q_1$, where Q_1 is the value of Q at R_1. The choice of ε_1 as a parameter reflects the fact that Q and not R is usually the fixed parameter in these experiments. An example for $\Gamma=9.002$ of the finite amplitude oscillations is given in Fig. 24, with each sequence corresponding to the labeled value of ε_1. If the frequency f, made dimensionless by a factor of t_v, is plotted versus ε_1 for many such sequences, Fig. 25(b) results; the solid curve is a least-squares fit giving $ft_v = 7.45\times10^{-2}\varepsilon_1^{1/2}$.

Although finite amplitude ("type II") periodicity occurs for most Γ's in the range $4 \lesssim \Gamma \lesssim 13$, there are a few values separated by $\Delta\Gamma \sim 1.1$ for which the amplitude A vanishes as $\varepsilon_1^{1/2}$ and the frequency remains nearly constant as $R \to R_1^+$. An example for $\Gamma=8.741$ showing how A vanishes in this case is given in Fig. 25(a) and labeled "type I." Here the solid curve is a least-squares fit giving $A = 4.04\times10^{-3}\varepsilon_1^{1/2} + 9.82\times10^{-3}\varepsilon_1^{3/2}$. By plotting the limiting amplitude as $R \to R_1^+$ vs Γ in Fig. 26, one can easily see the effect of the number of convection rolls in the container.

Since the usual conditions imposed in theoretical calculations require fixed R, rather than fixed Q, as in the experiments, a relevant question is whether the oscillations and indeed nearly all the observations of time dependence made with liquid helium are an artifact of the experimental method. This challenge to the experiments is particularly relevant because Busse (1967a) has provided calculations demonstrating the occurrence of finite amplitude oscillations as an artifact of a fixed-Q condition. Figure 27 demonstrates that the difference between a fixed Q and a fixed R is irrelevant to these experiments other than to

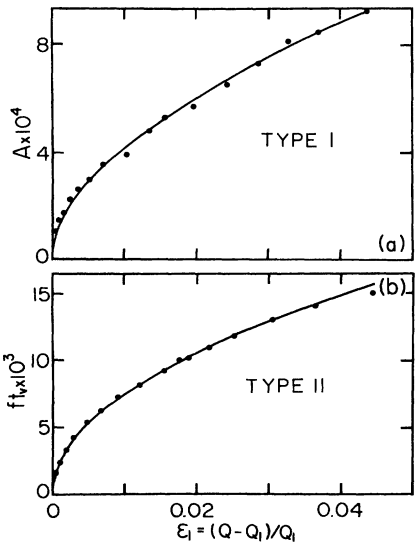

FIG. 25. (a) An example for $\Gamma=8.741$ showing the amplitude vanishing with the square root of the control parameter, here taken to be $\varepsilon_1=(Q-Q_1)/Q_1$. This occurs only for select aspect ratios separated by $\Delta\Gamma \simeq 1.1$ in the range $4 \lesssim \Gamma \lesssim 13$. (b) More typically, the amplitude remains nearly fixed and the frequency vanishes as $\varepsilon_1^{1/2}$. These frequencies were obtained from data selectively represented in Fig. 24 for $\Gamma=9.002$. See Behringer, Gao, and Shaumeyer (1983).

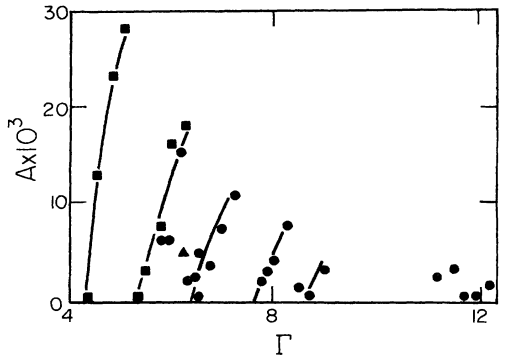

FIG. 26. The peak-to-peak amplitude A as $Q \to Q_1^+$ (from above) or $R \to R_1^+$ for periodic flows in the aspect-ratio range $4 \lesssim \Gamma \lesssim 13$. In this range of aspect ratios, the limiting value of A is usually nonzero. See Behringer, Gao, and Shaumeyer (1983).

provide an overall inversion of the signal. Figure 27(a) shows data taken under the usual conditions, with each run marked by the value of ε_1. Figure 27(b) shows data corresponding to the usual theoretical convention of fixed R; here runs are labeled by values of $(R - R_1)/R_1$.

An interesting question regards the physical origins of the transition at R_1. Some relevant information comes from recent experiments by Walden, Surko, Kolodner, and Passner (1983) involving water ($3 \lesssim \mathrm{Pr} \lesssim 5$) in a rectangular container with horizontal dimensions of nearly $10d \times 5 \times d$. Walden *et al.* found a hysteretic decrease in the number of convection rolls when the Rayleigh number exceeded values corresponding roughly to the skewed varicose instability. Since the experiments allow flow visualization, the wave number α was accessible. A reduction in the number of rolls decreases α and returns the system to the region of the stability diagram for which parallel rolls are stable (see Fig. 14). Indeed, sequences of pattern changes which decrease α with increasing R have been observed in other experiments, including recent ones by Croquette and Pocheau (1984), Steinberg, Ahlers and Cannell (1985) and older ones by Koshmieder (1966), Koshmieder and Pallas (1974), and Rossby (1969). Also, Gollub and Steinman (1981) observed the onset of noisy time dependence in a rectangular layer of water at the predicted onset of the skewed varicose instability.

For the helium experiments in cylindrical containers a mechanism relating to the skewed varicose instability may also play a role. However, there are a number of details which do not fit cleanly into such a simple picture. The value $R_1/R_c \sim 1.09$ which is found for large Γ corresponds for the skewed varicose instability to a wave number $\alpha = 3.46$, a value which is unaccountably large, given the critical wave number of $\alpha_c = 3.117$ at which the rolls are expected to form. In addition, no time dependence is expected on the basis of linear stability theory. Finally, no theory explains quantitatively why the presence of walls suppresses the skewed varicose instability at low aspect ratios although a pattern change still occurs.

At higher Rayleigh numbers where chaotic flow is well established, an interesting but unexplained feature for many experimental observations is the power spectra, typified by results of Ahlers and Behringer (1978a,1978b) in Fig. 28. Similar results have been observed by Gollub and Steinman (1981) for the local velocity in turbulent convecting water. Notable features are the flat low-frequency portion and the power-law falloff, $P(\omega) \sim \omega^{-a}$ at higher frequencies, where in the figure $f = \omega/2\pi$. Typically, the exponent a is $4 \pm \frac{1}{2}$. At very high Raleigh numbers studies of turbulent convection for low Pr are rather limited, although Threlfall (1975) has studied the

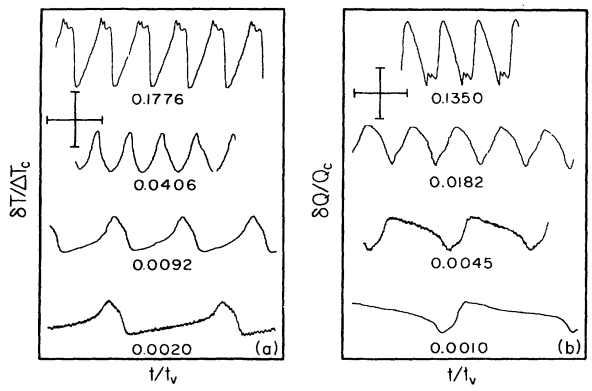

FIG. 27. An experimental demonstration of the equivalence of the fixed Q and the fixed R conditions (Gao and Behringer, 1984). (a) A sequence showing fluctuations $\delta T/\Delta T_c$ vs t/t_v at several values of ε_1 for $\Gamma = 7.923$. (b) A corresponding set of sequences for the same aspect ratio but showing dimensionless fluctuations in the heat flux $\delta Q/Q_c$ vs t/t_v at fixed R. Here Q_c is the value of the heat current Q at R_c and the number beneath each trace gives the appropriate value of $(R - R_1)/R_1$.

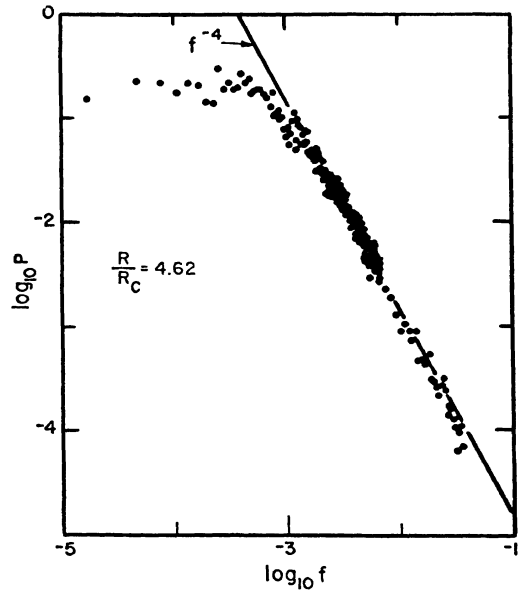

FIG. 28. The power P vs $f = \omega/2\pi$ for temperature fluctuations in a turbulent state, $R/R_c = 4.62$, for a cylindrical layer with $\Gamma = 4.72$ (Ahlers and Behringer, 1978a,1978b). The power falls off at higher frequencies as f^{-a} with $a = 4.0 + 0.2$.

heat transport in a turbulent layer of liquid helium.

A number of interesting questions clearly remain unresolved. In particular, the route to chaos followed by large-Γ systems is still unclear. The measurements of Gao and Behringer (1985) up to $\Gamma=22$ and Ahlers and Behringer (1978a,1978b) for $\Gamma=57$ show some fundamental differences. In no case has the existence of a strange attractor been determined for large layers. Although the physical origins of the onset of time-dependent flow at R_1 may be related to the skewed varicose instability, no quantitatively correct explanation currently exists. Relating the very precise thermal measurements available with liquid helium to the associated flow patterns is a considerable experimental challenge.

V. OTHER CONVECTIVE SYSTEMS

A. Introduction

Rayleigh-Bénard convection in a pure fluid represents one of the simplest examples of thermally driven flow. A number of related problems are also interesting, and some of these have been investigated using the sophistication of low-temperature techniques. Included are studies of convection in normal binary mixtures, a subject which has been reviewed in general by Schecter, Velarde, and Platten (1974) and by Gershuni and Zhukovitskii (1976), studies of convection in superfluid ^{3}He-^{4}He mixtures, and studies of convection in the presence of rotation. Due to the rich phase structure discussed in Sec. I, ^{3}He-^{4}He mixtures, when used in the normal phase, provide wide parameter ranges as well as the usual advantages in precision. The presence of the superfluid phase and the tricritical point provide new sorts of phenomena which are unique to liquid helium (Steinberg, 1981a,1981b; Fetter, 1981, 1982a,1982b). Each of the remaining sections gives a brief description of recent cryogenic work in the three areas of convection in normal mixtures ^{3}He-^{4}He mixtures, superfluid ^{3}He-^{4}He mixtures, and in the presence of rotation.

B. Normal ^{3}He-^{4}He mixtures

1. Equations of motion

A formal description of convection in nonreactive binary mixtures requires a number of modifications to the equations for a pure fluid (Landau and Lifshitz, 1959). Since two species exist, the continuity equation expressing conservation of total mass must be augmented by an additional equation which also guarantees conservation of each component. This new equation can be written in terms of the mass concentration c of component 1:

$$c=\frac{m_1 X}{m_1 X+m_2(1-X)} , \tag{84}$$

where X is the molar concentration, m_1 is the molar mass of component 1, and m_2 is the molar mass of component 2. The new conservation law is

$$\partial(\rho c)/\partial t=-\nabla\cdot(\rho c\mathbf{v})-\nabla\cdot\mathbf{i} , \tag{85}$$

where $\mathbf{i}$ is a diffusive concentration current defined below. To the quantities P,T providing a local thermodynamic description must be added an additional variable which may be taken as c.

A minor modification must also be made on the Navier-Stokes equations, Eqs. (15). Since the density in the buoyancy term $\rho\mathbf{g}$ may depend on c, T, and P, the effects of c must also be included. Again the pressure dependence of ρ is negligible, and the $\rho\mathbf{g}$ term may be approximated by

$$\rho\mathbf{g}=\rho_0\mathbf{g}[1-\alpha_{p,c}(T-T_0)-\beta_{P,T}(c-c_0)] , \tag{86}$$

where $\alpha_{p,c}=-\rho^{-1}\partial(\rho/\partial T)_{P,c}$ and $\beta_{P,T}=-\rho^{-1}\partial(\rho/\partial c)_{P,T}$. T_0 and c_0 are appropriate temperature and concentration reference values.

One final adjustment must be made to the entropy equation, since mass diffusion and heat flow provide irreversible mechanisms for increasing s. Indeed, these processes are linked; the irreversible heat flux $\mathbf{Q}$ and the mass diffusion current $\mathbf{i}$ are given by

$$\mathbf{i}=-\rho D[\nabla c+(k_T/T)\nabla T] \tag{87}$$

and

$$\mathbf{Q}=[k_T(\partial\mu/\partial c)_{P,T}-T(\partial\mu/\partial T)_{p,c}+\mu]\mathbf{i}-\kappa\nabla T . \tag{88}$$

A normally negligible term in ∇P has been omitted from $\mathbf{i}$, and the three quantities D, k_T, and μ have been introduced. These are the diffusion coefficient, the thermal diffusion ratio, and the chemical potential difference $\mu\equiv\mu_1-\mu_2$ defined in terms of the quantities

$$\mu_i=\partial\varepsilon/\partial(m_i N_i)\,|_{\rho,N_j\neq N_i} , \tag{89}$$

where N_i is the number of moles per volume of the ith component.

Referring to Fig. 5, the critical influence of the superfluid transition and the tricritical point causes dramatic variations in D and k_T, introducing a number of interesting phenomena (Steinberg, 1981a,1981b). As discussed from a theoretical viewpoint by Siggia and Nelson (1977) and from an experimental viewpoint by Behringer and Meyer (1982), D diverges at the superfluid transition, but vanishes at the tricritical point. The thermal diffusion ratio diverges strongly at the tricritical point, but diverges very weakly along the lambda line. By contrast to pure ^{4}He the measurable thermal conductivity, and the heat capacity $c_{p,c}$ are cusped but finite at the superfluid transition and are virtually unaffected by the tricritical point.

In terms of the currents $\mathbf{i}$ and $\mathbf{Q}$, the entropy equation becomes

$$\rho T(\partial s/\partial t+\mathbf{v}\cdot\nabla s)=\sum_{i,k}\sigma_{ik}\frac{\partial v_i}{\partial x_k}-\nabla\cdot(\mathbf{Q}-\mu\mathbf{i})-\mathbf{i}\cdot\nabla\mu . \tag{90}$$

Near the onset of convection the appropriate set of equations is, after one invokes the Boussinesq approximation,

$$\nabla\cdot\mathbf{v}=0\ , \tag{91}$$

$$\rho_0[\partial\mathbf{v}/\partial t+(\mathbf{v}\cdot\nabla)\mathbf{v}]=-\nabla P+\rho_0\mathbf{g}[1-\alpha_{p,c}(T-T_0)-\beta_{p,c}(c-c_0)]+\eta\nabla^2\mathbf{v}\ , \tag{92}$$

$$\partial c/\partial t+\mathbf{v}\cdot\nabla c=D[\nabla^2 c+(k_T/T)\nabla^2 T]\ , \tag{93}$$

$$\partial T/\partial t+\mathbf{v}\cdot\nabla T=(D_T+\mathscr{A}D)^2 T+(\mathscr{A}TD/k_T)\nabla^2 c\ . \tag{94}$$

Here D_T is modified to $D_T=\kappa/\rho c_{p,c}$ and $\mathscr{A}$ is a dimensionless parameter given by

$$\mathscr{A}=k_T^2(\partial\mu/\partial c)_{T,P}/c_{p,c}T\ . \tag{95}$$

2. Onset of convection

By introducing natural scale factors, such as d^2/D_T for time, it is possible to produce a set of dimensionless equations appropriate for convective flows and depending on the parameters $\mathscr{A}$, Pr, Sc, H, and R. These parameters are defined, after Lee, Lucas, and Tyler (1979,1983), by Eqs. (95) and (18) for $\mathscr{A}$ and Pr; R must be modified to

$$R=(\alpha_{p,c}g\,d^3\Delta T/\nu D_T)[(1+\mathscr{A})(1+S)+SD_T/T]\ , \tag{96}$$

with Sc, the modified Schmidt number, S, and H given by

$$\mathrm{Sc}=\nu/D(1+\mathscr{A})\ , \tag{97}$$

$$S=-\beta_{T,P}k_T/T\alpha_{p,c}\ , \tag{98}$$

and

$$H=\mathrm{Sc}S/\mathrm{Pr}(1+S)\ . \tag{99}$$

The choice of dimensionless parameters is far from unique. Indeed, a plethora of parameter sets has been used by different authors. We have chosen the present set for ease in discussing recent cryogenic experiments (Lee, Lucas, and Tyler, 1979,1983).

The coupling of the concentration and heat diffusion is readily apparent on constructing the simple z-dependent relaxational modes which are excited in response to temperature or concentration transients below the onset of convection. Following Behringer and Meyer (1982), these modes are characterized by zero velocity, with the remaining variables having a spatial dependence e^{iqz} and a relaxational time dependence $e^{-\sigma t}$ with $\sigma>0$. The equations of motion require the dispersion relations

$$\sigma q^2=D_{1,2}\ , \tag{100}$$

with

$$D_{1,2}^{-1}=\{D_T+D(1+\mathscr{A})\pm[(D_T+D(1+\mathscr{A}))^2-4DD_T]^{1/2}\}/2DD_T\ . \tag{101}$$

Note that when $\mathscr{A}=0$ (i.e., $k_T=0$), $D_{1,2}$ become D and D_T, and the resulting uncoupled modes correspond to strictly impurity or heat diffusion. The actual modes are usually characterized by $\mathscr{A}\neq 0$, and contain both temperature and concentration components. They can be calculated only by requiring appropriate conditions at the boundaries. The most common experimental conditions force $\mathbf{i}=0$ at $z=\pm\frac{1}{2}$, $T=0$ at $z=\frac{1}{2}$, and $Q=0$ at $z=-\frac{1}{2}$. When one invokes these constraints, the quantized rates σ must satisfy

$$\tan[d(\sigma/D_2)^{1/2}]/\tan[d(\sigma D_1)^{1/2}]=(D_1/D_2)^{1/2}(D_2-D)/(D_1-D)\ . \tag{102}$$

Recently this relation has been exploited (Behringer and Meyer, 1982) to obtain D for ^{3}He-^{4}He mixtures from measurements of σ and the remaining parameters contained in $D_{1,2}$. (See also Ahlers and Pobel, 1974.)

Following techniques similar to those described in Sec. II.B, one can use the linearized equations of motion to obtain the convective modes. As discussed by Schecter, Velarde, and Platten (1974), one of the most striking differences between a pure fluid and a mixture is the fact that convection may occur even when the density gradient is stabilizing. In addition, oscillations may accompany the onset of convection, a phenomenon known as overstability, and convection may occur when the layer is heated from either below or above, depending on the value of H. Recent calculations of R_c for the onset of static and overstable convection have been done by Lee, Lucas, and Tyler (1983) and by Gutkowicz-Krusin, Collins, and Ross (1979a,1979b). Here R_c is a function of H. Stability diagrams for the onset of steady convection with R_c now a function of H take the forms given by Lee, Lucas, and Tyler (1983) and are shown in Fig. 29 for the following regimes: I, $H<-1$ and $H>3.85$; II, $-1<H<0$; and III, $0<H<3.85$. The critical Rayleigh number corresponds to the lowest value of $|R(H,\alpha)|$; hence for case I and for case II when one is heating from above the onset of flow is predicted to occur for $\alpha=0$. Since experiments are done with finite Γ, the effect of the vertical boundaries should be important in these cases.

Lee, Lucas, Tyler, and Vavasour (1978) and Lee, Lucas, and Tyler (1979,1983) have recently used mixtures of ^{3}He and ^{4}He to test the stability theory for the onset of flow. Their results are summarized in Fig. 30, which gives their

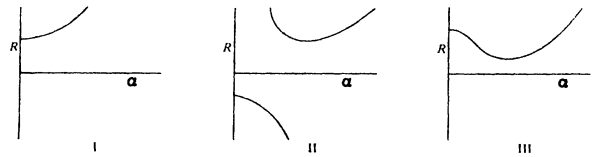

FIG. 29. Characteristic stability curves R vs α for binary mixtures with (I) $H<-1$ or $H>3.85$, (II) $-1<H<0$, (III) $0<H<3.85$, after Lee, Lucas, and Tyler (1983). H is defined by Eq. (99).

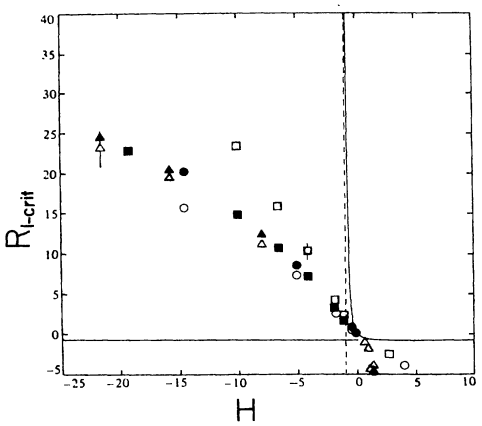

FIG. 30. Experimental values (open symbols) of $R_{1\,\mathrm{crit}}=-HR_c(H)/(1+H)$ vs H, for a cylindrical container with $\Gamma=6.25$ as well as the corresponding theoretical predictions for overstability in a horizontally infinite layer (solid symbols) and the onset of steady flow (solid curve). Circles, squares, and triangles correspond to ^{3}He molar concentrations of $X=0.016$, 0.079, and 0.134, respectively. These results are by Lee, Lucas, and Tyler (1983).

parameter $R_{1\,\mathrm{crit}}=-HR_c(H)/(1+H)$ as a function of H. Here R_c is the observed value of R at the onset of convection. The curve is the calculation for the onset of stationary convection, solid symbols are calculations for the onset of overstable convection, and the open symbols are experimental results for three different ^{3}He molar concentrations. Given the fairly large uncertainty in the fluid parameters, the agreement is generally good. In the liquid-helium experiments however, the phenomenon of overstability does not seem as well defined as in room-temperature experiments (Platten and Chavepeyer, 1973; Caldwell, 1974), and further experiments would be useful. Indeed, a characterization of flow in ^{3}He-^{4}He mixtures is only beginning. In general, stability calculations for $R>R_c$ comparable to those for a pure fluid have not been undertaken, and the onset of turbulence is virtually unexplored.

An interesting phenomenon for which ^{3}He-^{4}He mixtures may provide a useful test system occurs when H and R have been adjusted so that overstable and steady convection are both likely to occur. A discussion of this codimension-two problem (Guckenheimer and Holmes, 1983) has been given recently by Brand, Hohenberg, and Steinberg (1984).

C. Superfluid ^{3}He-^{4}He mixtures

Superfluidity occurs for temperatures below the lambda transition. Whereas liquid helium is a Newtonian fluid above the transition (i.e., in the normal phase), its properties in the superfluid phase are distinctly different. A phenomenological description of the hydrodynamics of a superfluid has been given by Landau and Lifshitz (1959) and Khalatnikov (1965). The fluid is to be viewed as an interpenetrating mixture of normal and superfluid components having velocities $\mathbf{v}_n$ and $\mathbf{v}_s$, so that the mass flux is

$$\mathbf{j}=\rho_n\mathbf{v}_n+\rho_s\mathbf{v}_s\ , \tag{103}$$

with the total density ρ given by

$$\rho=\rho_n+\rho_s\ . \tag{104}$$

The superfluid portion carries no entropy and flows irrotationally and without viscous drag, in contrast to the normal component, which like any conventional Newtonian fluid does carry entropy and experience viscous dissipation. At a more fundamental level, the normal fluid is associated with excitations on the superfluid ground state, and in a solution of ^{3}He and ^{4}He the ^{3}He molecules form a part of the normal fluid.

As in a normal mixture, energy, momentum, and the mass of each component must be conserved. Equation (105) provides for overall mass conservation:

$$\partial\rho/\partial t=-\nabla\cdot\mathbf{j}\ . \tag{105}$$

Due to the presence of two independent velocity fields, the dynamical equations for energy and momentum conservation, as given by Khalatnikov (1965), are considerably more complicated than those for a normal binary mixture, and accordingly they are not reproduced here. An additional phenomenological equation of motion describes the rate of change of $\mathbf{v}_s$:

$$\partial\mathbf{v}_s/\partial t+\nabla(\mu_4+1/2v_s^2)=\nabla[\zeta_3\nabla\cdot(\mathbf{j}-\rho\mathbf{v}_n)+\zeta_4\nabla\cdot\mathbf{v}_n]\ . \tag{106}$$

This relation expresses the expectations that $\nabla\times\mathbf{v}_s=0$ and that for small static gradients $\nabla\mu_4=0$. These equations provide a basis for describing a variety of unusual flow properties discussed in Wilks (1967). They also introduce a set of second viscosity coefficients ζ_1, ζ_2, ζ_3, and $\zeta_4=\zeta_1$ to allow for irreversible transport processes when both superfluid and normal motion exist.

Several authors, including Steinberg (1981a,1981b), Steinberg and Brand (1983), and Fetter (1981, 1982a,1982b), have used this description of superfluid flow to study the onset of convection. As in simpler systems, the preconvecting state is determined and its stability to perturbations is tested. However, this state is not characterized by $\mathbf{v}_n=\mathbf{v}_s=0$. Rather, there exists a one-dimensional counterflow of $\mathbf{v}_n$ and $\mathbf{v}_s$ with $\mathbf{j}=0$; the concentration balance is maintained through the diffusive mass flux given in Eq. (87). Because this state is characterized, when the effect of gravity is negligible, by $\nabla P=\nabla\mu_4=0$, gradients in any remaining thermodynamic variables, such as c or s, depend only on ∇T. In this case, the experimentally observed effective conductivity and effective thermal diffusion ratio are related simply to thermodynamic quantities:

$$\kappa_{\mathrm{eff}}=\kappa+\rho DT(\partial\mu/\partial c)^{-1}[c\partial(s/\rho c)\partial c+(k_T/T)\partial\mu/\partial c]^2\ , \tag{107}$$

and

$$k_T^* = c\partial(s/\rho c)/\partial c \mid_{p,\mu_4} . \quad (108)$$

A linearization about the preconvective state after suitable (although not unique) dimensional analysis yields a set of non-self-adjoint equations for the convective modes. Dimensionless parameters entering the equations include a new Rayleigh number,

$$R = \alpha_{\mu_4,p} g\, d^3 \Delta T / D_{T\,\mathrm{eff}} \nu_n , \quad (109)$$

a redefined Prandtl number,

$$\mathrm{Pr} = \nu_n / D_{T\,\mathrm{eff}} , \quad (110)$$

$$m = (\zeta_1 - \rho\zeta_3)/\nu_n , \quad (111)$$

$$\varepsilon_1 = -v_{nz}^0 , \quad (112)$$

$$\varepsilon_2 = \gamma \Delta T / T , \quad (113)$$

$$\varepsilon_3 = (\rho/\rho_n) g\, d\beta_{c,p} m / \mid (\partial\mu_4/\partial c)_{T,P} \mid , \quad (114)$$

and

$$\gamma = -(\partial \ln c / \partial \ln T)_{\mu_4,p} . \quad (115)$$

Here $\alpha_{\mu_4,p}$ is the expansion coefficient at constant μ_4 and P, $\nu_n = \eta/\rho_n$, $D_{T\,\mathrm{eff}} = \kappa_{\mathrm{eff}}/\rho c_{p,c}$, and the superscript 0 refers to the preconvective state. The set of parameters m, γ, ε_1, ε_2, and ε_3 occurs only in the superfluid problem. If they are zero, the linearized stability problem is identical in form to that for a pure normal fluid. Noting this property, Fetter (1982a) has performed a perturbation analysis to obtain the critical Rayleigh number when these parameters are small, which is the case for the experiments described below. He finds for a horizontally infinite layer that

$$R_c = R_{c0} + 24.6\varepsilon_1\varepsilon_2 + 10.2(\varepsilon_1 - \varepsilon_2)^2 - 19.9\varepsilon_2(\varepsilon_1\rho/\rho_s - \varepsilon_3) + \cdots , \quad (116)$$

where $R_{c0} = 1707.76\ldots$ is the value of R_c for a pure normal fluid.

Experiments have been made by Warkentin, Haucke, and Wheatley (1980) and Warkentin, Haucke, Lucas, and Wheatley (1980) near the onset of superfluid convection. Using a $\Gamma = 1$ cylindrical cell, they found $R_c = 1708$. This result is somewhat lower than expected, since Fetter (1982a,1982b) and Steinberg and Brand (1983) claim that the critical Rayleigh number for this geometry should be nearly equal to 2660, the value which would be obtained in a pure normal fluid with $\Gamma = 1$. The discrepancy between theory and experiment remains unresolved, although Steinberg and Brand (1983) have suggested that spatial variations in μ_4 which were neglected in existing calculations may play a role. However, given the uncertainty in the parameters determining R, the agreement is not too bad.

Recent experiments by Maeno, Haucke, Ecke, and Wheatley (1984), Maeno, Haucke, and Wheatley (1985), and Ecke, Maeno, Haucke, and Wheatley (1984) have pursued the analogy of convection in a superfluid mixture to that in a pure fluid by studying the onset of the oscillatory instability. (See also Haucke *et al.*, 1984.) For low Prandtl number pure (normal) fluids, exemplified by mercury with $\mathrm{Pr} = 0.026$, the stability calculations of Clever and Busse (1974) indicate that the oscillatory instability (see Sec. III.E) is the first instability encountered as R increases above R_c. No corresponding calculations exist for superfluid mixtures; however, their Prandtl number may be adjusted over the range $0.02 < \mathrm{Pr} < 3.0$. Accordingly an interesting question regards the occurrence of similar oscillations in a superfluid mixture. It is this question which Maeno, Haucke, and Wheatley have addressed using a rectangular cell of dimensions $2.0d : 1.4d : d$. Figure 31 shows the rms values of the observed periodic oscillations in ΔT near onset at fixed heat flux, and the corresponding region of the Nusselt number curve, both versus ε. The linear initial rise of the rms fluctuations δT is an interesting feature. Another interesting set of results is given in Fig. 32, where ε_0, the value of ε at the onset of oscillations, is given versus Pr. Theory for a pure normal fluid (Clever and Busse, 1974) indicates such a linear change with Pr, although the observed values of ε_0 are larger than those expected for a pure normal fluid with $\Gamma = \infty$. In the present case the experiments suggest intriguing similarities to a pure fluid, although there is not yet sufficient knowledge of the hydrodynamic solutions to provide adequate comparison, nor are there yet sufficient experimental data to reveal dependence, if any, on the aspect ratio and the wave number of the steady flow.

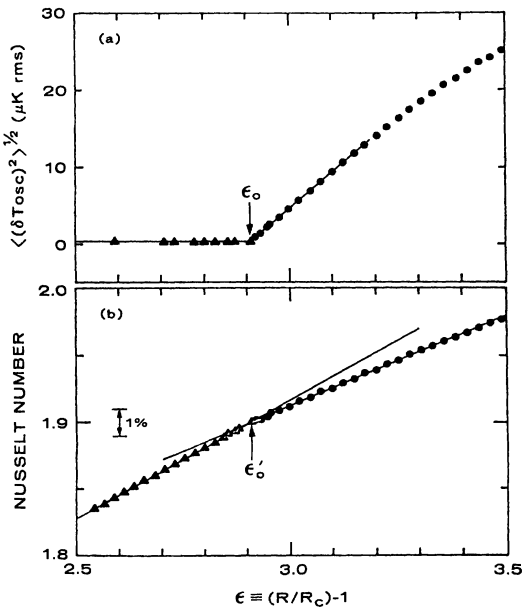

FIG. 31. (a) The rms values of the periodic temperature variations δT at fixed heat current Q vs ε in a superfluid ^{3}He-^{4}He mixture, after Maeno, Haucke, and Wheatley (1984). (b) The corresponding effect on the Nusselt number. The value of ε observed for the onset of oscillations is indicated by ε_0 and ε_0'.

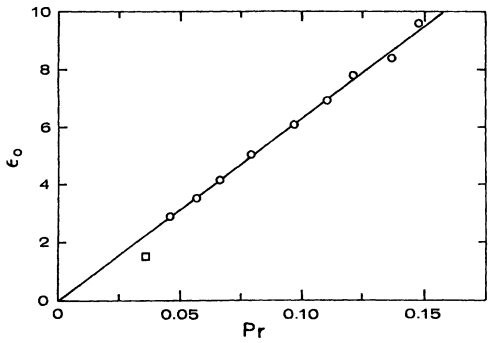

FIG. 32. Values of ε_0, the value of ε at the onset of periodic flow, vs Prandl number Pr for superfluid mixtures, after Maeno, Haucke, and Wheatley (1984).

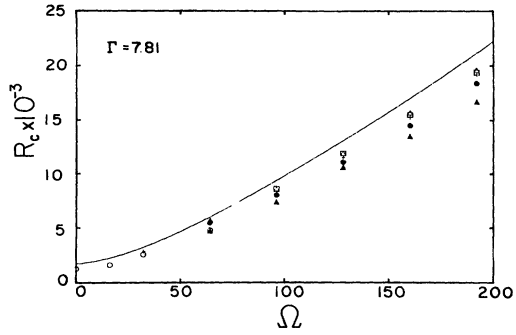

FIG. 33. Values of $R(\Omega)$ vs the dimensionless angular velocity Ω for a rotating layer of liquid helium with $\Gamma=7.81$ (Pfotenhauer, 1984; Lucas, Pfotenhauer, and Donnelly, 1983). The solid line gives $R_c(\Omega)$ for a horizontally infinite layer (Chandrasekhar, 1961).

D. Convection with rotation

The last area in which cryogenic techniques have been applied involves a convecting layer of pure fluid where the boundaries are rotated about a vertical axis. The rate of rotation is ω, and a new dimensionless parameter, $\Omega=\omega d^2/\nu$, enters the problem. A convenient description involves transforming to a frame rotating with the boundaries. In the rotating frame the noninertial centrifugal and Coriolis forces appear directly in modified Navier-Stokes equations:

$$\rho[\partial \mathbf{v}/\partial t+(\mathbf{v}\cdot\nabla)\mathbf{v}]=-\nabla P+\rho\mathbf{g}-\rho\boldsymbol{\omega}\times(\boldsymbol{\omega}\times\mathbf{r}) -\rho\boldsymbol{\omega}\times\mathbf{v}+\eta\nabla^2\mathbf{v}\ . \quad (117)$$

Of these only the Coriolis force, which tends to inhibit convection, is usually important, since the centrifugal force is usually small compared to the force of gravity.

Experimental work on rotating convecting layers is relatively sparse compared to work on nonrotating layers. Results in room-temperature fluids have been obtained by Nakagawa and Frenzen (1955), Fultz and Nakagawa (1955), Dropkin and Globe (1959), Goroff (1960), Rossby (1969), and Krishnamurti (1971). Most recently, Lucas, Pfotenhauer, and Donnelly (1981,1983) and Pfotenahuer (1984) have presented results using liquid ^{4}He as the rotating fluid. This work is also discussed in the review article by Pfotenhauer and Donnelly (1984).

Recent theoretical work includes Küppers and Lortz (1969), Küppers (1970), Clever and Busse (1979), Busse (1981), and Buell and Catton (1983a,1983b).

The onset of convection occurs at a Rayleigh number R_c which depends only on Ω and the geometry of the convecting layer. Calculations of R_c for straight parallel rolls were made originally by Chandrasekhar (1961) for a horizontally infinite layer. Recently Buell and Catton (1983a,1983b) have calculated R_c for a cylindrically confined layer with aspect ratios $\Gamma \lesssim 2$. An interesting feature of this last work is that nonaxisymmetric modes may have lower values of R_c than axisymmetric modes.

Experimental determinations of $R_c(\Omega)$, after Lucas, Pfotenhauer, and Donnelly (1983) and Pfotenhauer (1984) are shown in Fig. 33. In this work, ^{4}He was used in a variety of cylindrical containers with aspect ratios 1.97, 3.22, 4.93, and 7.81. The present results for $\Gamma=7.81$ show agreement with the infinite layer calculations (Chandrasekhar, 1961) within the errors of the fluid parameter needed to calculate R, given ΔT. Pfotenhauer (1984) and Lucas, Pfotenhauer, and Donnelly (1983) have also documented the suppression of the convective amplitude with increasing Ω using liquid helium. Shown in Fig. 34 are their results for the Nusselt number $N(R)$ for several values of Ω. The suppression of the convection, as manifested through the slope $M=dN/dR$, as well as R_c, is clear. (Here it is important to distinguish M from the parameter $S=R_cM$.) An interesting feature of the last figure is the tendency for convection to begin at an apparent subcritical Rayleigh number. The authors have argued in reference to Buell and Catton (1983b) that this result is attributable to the onset of nonaxisymmetric flow.

A relatively unexplored area for experiments involves the onset of time-dependent flow. Küppers and Lortz (1969) and Küppers (1970) showed that for $\Omega \gtrsim \Omega_c=24$

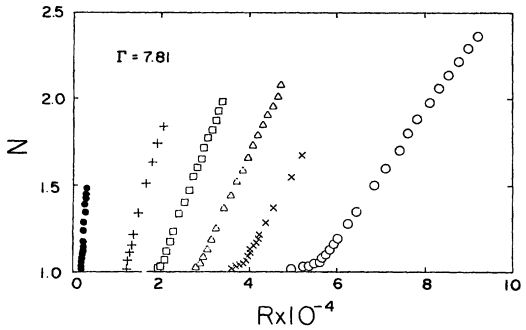

FIG. 34. Nusselt number N as a function of R at several values of Ω for a $\Gamma=7.81$ cylindrical layer of liquid ^{4}He (Pfotenhauer, 1984; Lucas, Pfotenhaur, and Donnelly, 1983). The values of Ω are as follows: solid circles, $\Omega=0$; +, $\Omega=128$; squares, $\Omega=192$; triangles, $\Omega=256$; ×, $\Omega=320$; open circles, $\Omega=452$.

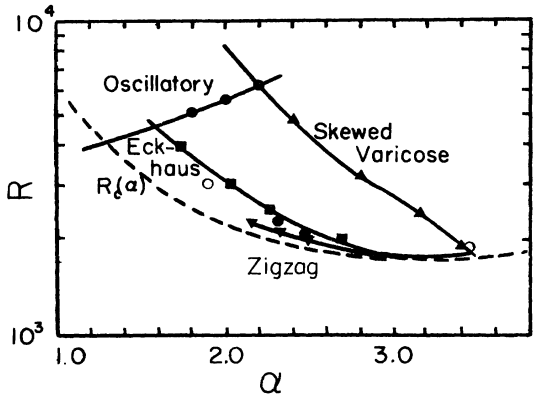

FIG. 35. The theoretically obtained diagram for a rotating horizontally infinite layer with Pr=0.71 and $\Omega=5$ (Clever and Busse, 1979). This figure should be compared to Fig. 13 corresponding to $\Omega=0$.

($R=\infty$, slip walls) no steady convective solutions exist for a horizontally unbounded layer, although they did not determine the nature of the resulting time dependence. Clever and Busse (1979) and Busse (1981) have reinvestigated the Küppers-Lortz instability in the context of an overall stability analysis. They find for small Ω that parallel rolls have the same types of instabilities as a nonrotating layer. Figure 35 gives their stability diagram for $P=0.71$ and $\Omega=5$. These authors predict that for $\Omega=10$, the domain of stability for parallel rolls with Pr=0.71 is practically nonexistent. Clever and Busse (1979) and Busse (1981) have also investigated the time dependence which develops above the Küppers-Lortz instability. According to their nonlinear calculations, this time dependence consists of three sets of crossed rolls forming a hexagonal pattern, with the maximum amplitude alternating among the three sets. Motion is sustained as the result of statistical noise present in the layer.

To date, no clear experimental verification of this sort of time dependence or the route to turbulence exists from either cryogenic or room-temperature experiments, although Krishnamurti (1971) has observed hexagonal patterns in the presence of rotation.

VI. SUMMARY AND FUTURE DIRECTIONS

Recent experiments using liquid helium have provided a quantitative test of specific predictions concerning steady and turbulent convective flows. The main advantages of cryogenic experiments are their high precision, their ability to follow changes associated with an evolving flow easily and with high sensitivity, and their unique range of available Prandtl numbers. Both the amplitude and time evolution to steady flows are generally in agreement with theory. A characterization of flow patterns in liquid helium remains an experimental challenge which becomes more important in light of recent theoretical descriptions of pattern evolution.

Through studies in a variety of different geometries, helium experiments in concert with those at room temperatures have verified a number of recent theoretical predictions and scenarios for the evolution of turbulence. Among the scenarios are turbulence via intermittency, via a period-doubling cascade, and via a multiply periodic state involving a small number of fundamental frequencies. The cryogenic measurements have particularly demonstrated the importance of geometry to the onset of turbulent flow. They have also provided a bridge between work done at very small aspect ratios where only a very few modes are relevant, and work pertaining to large aspect ratios where calculations for horizontally infinite layers are likely to pertain. For at least moderately large aspect-ratio cylindrical layers, the onset of time dependence is not in quantitative agreement with stability calculations by Clever and Busse for the skewed varicose instability. The resolution of this issue remains an interesting problem. Likewise, the onset of turbulence in very large layers is a subject of continuing study. Existing measurements for a $\Gamma=57$ cylindrical layer have shown turbulent behavior quite close to R_c, whereas other measurements up to $\Gamma=22$ show a time-independent convective regime followed by a route to turbulence over a fairly narrow region in R/R_c. The seeming contradiction between the two sets of data may be resolved by the theory of Cross and Newell (1984). Further experimental work is clearly in order.

An important point regarding emerging theories of turbulence is their broad applicability to many different dynamical systems. In this regard, experiments using mixtures of ^{3}He and ^{4}He—both normal and superfluid—as well as rotating helium experiments, are likely to provide a rich testing ground for theory. Current experiments for the first and last of these systems have focused chiefly on the static flow properties. An understanding of what is probably the most intriguing aspect of these systems, the onset of turbulence, is yet to come.

ACKNOWLEDGMENTS

I am grateful to Professor Guenther Ahlers and to Professor Russell Donnelly for detailed comments on this work, which was supported by the National Science Foundation under Low-Temperature Physics Grant No. DMR-8314673 and by an Alfred P. Sloan Foundation Fellowship.

REFERENCES

Abraham, N. B., J. P. Gollub, and H. L. Swinney, 1984, Physica D **11**, 252.
Ahlers, G., 1968, Phys. Rev. Lett. **21**, 1159.
Ahlers, G., 1974, Phys. Rev. Lett. **33**, 1185.
Ahlers, G., 1975, in *Fluctuations, Instabilities, and Phase Transitions*, edited by T. Riste (Plenum, New York), p. 181.
Ahlers, G., 1976, in *The Physics of Liquid and Solid Helium, Part I*, edited by K. H. Bennemann and J. B. Ketterson (Wiley, New York), p. 85.

Ahlers, G., 1980a, in *Systems Far from Equilibrium*, edited by L. Garrido, Lecture Notes in Physics (Springer, Berlin), Vol. 132, p. 143.
Ahlers, G., 1980b, J. Fluid Mech. **98**, 137.
Ahlers, G., and R. P. Behringer, 1978a, Phys. Rev. Lett. **40**, 712.
Ahlers, G., and R. P. Behringer, 1978b, Prog. Theor. Phys. Suppl. **64**, 186.
Ahlers, G., and R. P. Behringer, 1979, unpublished.
Ahlers, G., M. C. Cross, P. C. Hohenberg, and S. Safran, 1981, J. Fluid Mech. **110**, 297.
Ahlers, G., P. C. Hohenberg, and M. Lucke, 1985, Phys. Rev. Lett. **53**, 48.
Ahlers, G., P. C. Hohenberg, and M. Lucke, 1985, preprint.
Ahlers, G., and F. Pobel, 1974, Phys. Rev. Lett. **32**, 144.
Ahlers, G., and R. W. Walden, 1980, Phys. Rev. Lett. **44**, 445.
Barenghi, C. F., P. Lucas, and R. J. Donnelly, 1981, J. Low Temp. Phys. **44**, 491.
Behringer, R. P., C. Agosta, J. S. Jan, and J. M. Shaumeyer, 1980, Phys. Lett. **80A**, 273.
Behringer, R. P., and G. Ahlers, 1977, Phys. Lett. **62A**, 329.
Behringer, R. P., and G. Ahlers, 1982, J. Fluid Mech. **125**, 219.
Behringer, R. P., H. Gao, and J. N. Shaumeyer, 1983, Phys. Rev. Lett. **50**, 1199.
Behringer, R. P., and H. Meyer, 1982, J. Low Temp. Phys. **46**, 407.
Behringer, R. P., J. N. Shaumeyer, C. A. Clark, and C. C. Agosta, 1982, Phys. Rev. A **26**, 3723.
Bénard, H., 1901, Ann. Chim. Phys. **7**, Ser. 23, 62.
Bergé, P., 1975, in *Fluctuations, Instabilities, and Phase Transitions*, edited by T. Riste (Plenum, New York), p. 323.
Bergé, P., and M. Dubois, 1974, Phys. Rev. Lett. **32**, 1041.
Bergé, P., M. Dubois, P. Manneville, and Y. Pomeau, 1980, J. Phys. (Paris) Lett. **41**, 341.
Bolton, E. W., F. H. Busse, and R. M. Clever, 1983, Bull. Am. Phys. Soc. **28**, 1399.
Boussinesq, J., 1903, *Theorie Analytique de la Chaleur* (Gauthier-Villars, Paris), Vol. 2.
Brand, H. R., P. C. Hohenberg, and V. Steinberg, 1984, Phys. Rev. A **30**, 2548.
Buckingham, M. J., and W. M. Fairbank, 1961, in *Progress in Low Temperature Physics*, edited by C. J. Gorter (North-Holland, Amsterdam), Vol. III, p. 80.
Buell, Jeffrey C., and I. Catton, 1983a, Phys. Fluids **26**, 892.
Buell, J. C., and I. Catton, 1983b, J. Heat Transfer **105**, 255.
Busse, F. H., 1967a, J. Fluid Mech. **28**, 232.
Busse, F. H., 1967b, J. Fluid Mech. **30**, 625.
Busse, F. H., 1978, Rep. Prog. Phys. **41**, 1929.
Busse, F. H., 1981, in *Hydrodynamic Instabilities and the Transition to Turbulence*, edited by H. L. Swinney and J. P. Gollub (Springer, Berlin), p. 97.
Busse, F. H., and R. M. Clever, 1979, J. Fluid Mech. **91**, 319.
Caldwell, D. R., 1974, J. Fluid Mech. **64**, 347.
Chandrasekhar, S., 1961, *Hydrodynamic and Hydromagnetic Stability* (Oxford, London).
Charlson, G. S., and R. L. Sani, 1970, Int. J. Heat Mass Transfer **13**, 1479.
Charlson, G. S., and R. L. Sani, 1971, Int. J. Heat Mass Transfer **14**, 2157.
Clever, R. M., and F. H. Busse, 1974, J. Fluid Mech. **65**, 625.
Croquette, V., M. Mory, and F. Schosseler, 1983, J. Phys. (Paris) **44**, 293.
Croquette, V., and A. Pocheau, 1984, *Lecture Notes in Physics* (Springer, Berlin), Vol. 210, p. 104.
Cross, M. C., 1980, Phys. Fluids **23**, 1727.
Cross, M. C., 1982, Phys. Rev. A **25**, 1065.
Cross, M. C., P. G. Daniels, P. C. Hohenberg, and E. D. Siggia, 1980, Phys. Rev. Lett. **45**, 898.
Cross, M. C., P. G. Daniels, P. C. Hohenberg, and E. D. Siggia, 1983, J. Fluid Mech. **127**, 155.
Cross, M. C., and A. C. Newell, 1984, Physica D **10**, 299.
Daniels, P. G., 1977, Proc. R. Soc. London, Ser. A **358**, 173.
Daniels, P. G., 1978, Mathematika **25**, 216.
Dropkin, D., and S. Globe, 1959, J. Appl. Phys. **30**, 84.
Dubois, M., M. A. Rubio, and P. Bergé, 1983, Phys. Rev. Lett. **51**, 1446.
Ecke, R. E., Y. Maeno, H. Haucke, and J. C. Wheatley, 1984, Phys. Rev. Lett. **53**, 1567.
Eckhaus, W., 1965, *Studies in Non-Linear Stability Theory* (Springer, Berlin).
Eckmann, J. P., 1981, Rev. Mod. Phys. **53**, 643.
Farmer, J. D., E. Ott, and J. A. Yorke, 1983, Physica D **7**, 153.
Feigenbaum, M. J., 1978, J. Stat. Phys. **19**, 25.
Feigenbaum, M. J., 1979, Phys. Lett. **74A**, 375.
Fetter, A. L., 1981, Physica B **107**, 149.
Fetter, A. L., 1982a, Phys. Rev. B **26**, 1164.
Fetter, A. L., 1982b, Phys. Rev. B **26**, 1174.
Fultz, D., and Y. Nakagawa, 1955, Proc. R. Soc. London, Ser. A **231**, 211.
Gao, H., and R. P. Behringer, 1984, Phys. Rev. A **30**, 2837.
Gao, H., G. Metcalfe, T. Jung, and R. P. Behringer, 1985, to appear.
Gershuni, G. Z., and E. M. Zhukovitskii, 1976, *Convective Stability of Incompressible Fluids* (Israel Program for Scientific Translations, Jerusalem).
Gollub, J. P., and S. V. Benson, 1980, J. Fluid Mech. **100**, 449.
Gollub, J. P., S. V. Benson, and J. Steinman, 1980, Ann. N.Y. Acad. Sci. **357**, 22.
Gollub, J. P., and M. S. Heutmaker, 1984, in *Turbulence and Chaotic Phenomena in Fluids*, edited by T. Tatsumi (North-Holland, Amsterdam),
Gollub, J. P., A. R. McCarriar, and J. F. Steinman, 1982, J. Fluid Mech. **125**, 259.
Gollub, J. P., and J. F. Steinman, 1981, Phys. Rev. Lett. **47**, 505.
Gorman, M., L. A. Reith, and H. L. Swinney, 1980, Ann. N.Y. Acad. Sci. **357**, 10.
Gorman, M., P. J. Widmann, and K. A. Robbins, 1984, Phys. Rev. Lett. **52**, 2241.
Goroff, I., 1960, Proc. R. Soc. London, Ser. A **254**, 537.
Graham, R., 1974, Phys. Rev. A **10**, 1762.
Grassberger, P., and I. Procaccia, 1983a, Phys. Rev. Lett. **50**, 346.
Grassberger, P., and I. Procaccia, 1983b, Physica D **9**, 189.
Gray, D. D., and A. Giorgini, 1976, Int. J. Heat Mass Transfer **99**, 545.
Grebogi, C., E. Ott, and J. A. Yorke, 1983, Phys. Rev. Lett. **51**, 339.
Greenside, H. S., W. M. Coughran, and N. L. Schryer, 1982, Phys. Rev. Lett. **49**, 726.
Greenside, H. S., and W. M. Coughran, Jr., 1984, Phys. Rev. A **30**, 398.
Guckenheimer, J., and P. Holmes, 1983, *Nonlinear Oscillations, Dynamical Systems and Bifurcations of Vector Fields* (Springer, Berlin).
Guckenheimer, J., and R. F. Williams, 1976, Appl. Math. Sci. **19**, 368.
Gutkowicz-Krusin, D., M. A. Collins, and J. Ross, 1979a, Phys.

Fluids **22**, 1443.
Gutkowicz-Krusin, D., M. A. Collins, and J. Ross, 1979b, Phys. Fluids **22**, 1451.
Hall, P., and I. C. Walton, 1977, Proc. R. Soc. London, Ser. A **358**, 199.
Haucke, H., and Y. Maeno, 1983, Physica D **7**, 69.
Haucke, H., Y. Maeno, P. Warkentin, and J. Wheatley, 1981, J. Low Temp. Phys. **44**, 505.
Haucke, H., R. E. Ecke, Y. Maeno, and J. C. Wheatley, 1984, Phys. Rev. Lett. **53**, 2090.
Hill, R. W., and O. V. Lounasmaa, 1957, Philos. Mag. **2**, 143.
Hill, R. W., and O. V. Lounasmaa, 1960, Proc. R. Soc. London, Ser. A **252**, 357.
Hirsch, M. W., and S. Smale, 1974, *Differential Equations, Dynamical Systems, and Linear Algebra* (Academic, New York).
Hopf, E., 1948, Commun. Pure Appl. Math. **1**, 303.
Joseph, D. D., 1976, *Stability of Fluid Motions I/II* (Springer, Berlin).
Kaplan, J. L., and J. A. Yorke, 1979, Ann. N.Y. Acad. Sci. **316**, 400.
Keller, W. E., 1969, *Helium-3 and Helium-4* (Plenum, New York).
Kelly, R. E., and D. Pal, 1978, J. Fluid Mech. **86**, 433.
Khalatnikov, I. M., 1965, *An Introduction to the Theory of Superfluidity* (Benjamin, New York).
Koschmieder, E. L., 1966, Beitr. Phys. Atmos. **39**, 1.
Koschmieder, E. L., 1974, Adv. Chem. Phys. **26**, 177.
Koschmieder, E. L., and S. G. Pallas, 1974, Int. J. Heat Mass Transfer **17**, 991.
Krishnamurti, R., 1971, in *Naval Hydrodynamics,* Eighth Symposium, edited by M. S. Plesset, T. Y.-T. Wu, and S. W. Doroff, report ARC-179, p. 289.
Küppers, G., 1970, Phys. Lett. **32A**, 7.
Küppers, G., and D. Lortz, 1969, J. Fluid Mech. **35**, 609.
Landau, L. D., and E. M. Lifshitz, 1959, *Fluid Mechanics* (Pergamon, Oxford).
Lee, G., P. G. J. Lucas, and A. Tyler, 1979, Phys. Lett. **75A**, 81.
Lee, G. W. T., P. G. J. Lucas, and A. Tyler, 1983, J. Fluid Mech. **135**, 235.
Lee, G., P. G. J. Lucas, A. Tyler, and E. Vavasour, 1978, J. Phys. (Paris) Colloq. **39**, C6-178.
Libchaber, A., 1983, Physica B **109&110**, 1583.
Libchaber, A., S. Fauve, and C. LaRoche, 1983, Physica D **7**, 73.
Libchaber, A., and J. Maurer, 1978, J. Phys. (Paris) Lett **39**, 369.
Libchaber, A., and J. Maurer, 1980, J. Phys. (Paris) Colloq. **41**, C3-51.
Lucas, P. G. J., J. M. Pfotenhauer, and R. J. Donnelly, 1981, Physica B **107**, 147.
Lucas, P. G. J., J. M. Pfotenhauer, and R. J. Donnelly, 1983, J. Fluid Mech. **129**, 251.
Lorenz, E. N., 1963, J. Atm. Sci. **20**, 130.
Maeno, Y., H. Haucke, R. E. Ecke, and J. C. Wheatley, 1984, LT-17, 1123.
Maeno, Y., H. Haucke, and J. C. Wheatley, 1985, Phys. Rev. Lett. **54**, 340.
Manneville, P., and Y. Pomeau, 1979, Phys. Lett. **75A**, 1.
Manneville, P., and Y. Pomeau, 1980, Physica D **1**, 219.
Maurer, J., and A. Libchaber, 1980, J. Phys. (Paris) Lett. **41**, 515.
May, R. M., 1976, Nature **261**, 459.
McLaughlin, J. B., and P. C. Martin, 1974, Phys. Rev. Lett. **33**, 1189.
McLaughlin, J. B., and P. C. Martin, 1975, Phys. Rev. A **12**, 186.
Moore, D. R., and N. O. Weiss, 1973, J. Fluid Mech. **61**, 553.
Mueller, K. H., G. Ahlers, and F. Pobell, 1976, Phys. Rev. B **14**, 2096.
Musman, S., 1968, J. Fluid Mech. **31**, 343.
Nakagawa, Y., and P. Frenzen, 1955, Tellus **7**, 1.
Newell, A. C., and J. A. Whitehead, 1969, J. Fluid Mech. **38**, 279.
Newhouse, S., D. Ruelle, and F. Takens, 1978, Commun. Math. Phys. **64**, 35.
Normand, C., Y. Pomeau, and M. Velarde, 1977, Rev. Mod. Phys. **49**, 581.
Oberbeck, A., 1879, Ann. Phys. Chem. **7** (new series), 271.
Otnes, R. K., and L. Enochson, 1972, *Digital Time Series Analysis* (Wiley, New York).
Ott, E., 1981, Rev. Mod. Phys. **53**, 655.
Packard, N. H., J. P. Crutchfield, J. D. Farmer, and R. S. Shaw, 1980, Phys. Rev. Lett. **45**, 712.
Pfotenhauer, J. M., 1984, Ph.D. thesis (University of Oregon).
Pfotenhauer, J. M., and R. J. Donnelly, 1985, to appear in Adv. Heat Transfer, edited by J. P. Harnett and T. Irvine, Vol. 17.
Platten, J. K., and G. Chavepeyer, 1973, J. Fluid Mech. **60**, 305.
Pomeau, Y., and P. Manneville, 1979, J. Phys. (Paris) Lett. **40**, 609.
Pomeau, Y., and P. Manneville, 1981, J. Phys. (Paris) **42**, 1067.
Pomeau, Y., and S. Zaleski, 1981, J. Phys. (Paris) **42**, 515.
Rayleigh, Lord J. W. S., 1916, Philos. Mag. **32**, 529.
Rossby, H. T., 1969, J. Fluid Mech. **36**, 309.
Roux, J. C., R. H. Simoyi, and H. L. Swinney, 1983, Physica D **8**, 257.
Ruelle, D., and F. Takens, 1971, Commun. Math. Phys. **20**, 167.
Saltzman, B., 1962, Int. J. Atmos. Sci. **19**, 329.
Sano, M., and Y. Sawada, 1978, Prog. Theor. Phys. (Kyoto), Suppl. **64**, 202.
Schecter, R. S., M. G. Velarde, and J. K. Platten, 1974, Adv. Chem. Phys. **26**, 265.
Schlüter, A., D. Lortz, and F. Busse, 1965, J. Fluid Mech. **23**, 129.
Segel, S. A., 1969, J. Fluid Mech. **38**, 203.
Shaumeyer, J. N., and R. P. Behringer, 1981, unpublished.
Shaumeyer, J. N., R. P. Behringer, and R. Baierlein, 1981, J. Fluid Mech. **109**, 339.
Siggia, E. D., and D. R. Nelson, 1977, Phys. Rev. B **15**, 1427.
Steinberg, V., 1981a, Physica B **107**, 151.
Steinberg, V., 1981b, Phys. Rev. A **24**, 2584.
Steinberg, V., G. Ahlers, and D. S. Cannell, 1985, Phys. Scr. **T9**, 97.
Steinberg, V., and H. R. Brand, 1983, Phys. Rev. B **28**, 1618.
Stuart, J. T., and R. C. DiPrima, 1978, Proc. R. Soc. London, Ser. A **362**, 27.
Swift, J., and P. C. Hohenberg, 1977, Phys. Rev. A **15**, 319.
Swinney, H. L., 1983, Physica D **7**, 3.
Threlfall, D. C., 1975, J. Fluid Mech. **67**, 17.
Tough, J. T., 1982, in *Progress in Low Temperature Physics,* edited by D. F. Brewer (North-Holland, Amsterdam), Vol. VIII, p. 133.
Walden, R. W., 1983, Phys. Rev. A **27**, 1255.
Walden, R. W., and G. Ahlers, 1981, J. Fluid Mech. **109**, 89.
Walden, R. W., P. Kolodner, A. Passner, and C. M. Surko, 1984, Phys. Rev. Lett. **53**, 242.

Walden, R. W., S. Surko, P. Kolodner, and A. Passner, 1983, Bull. Am. Phys. Soc. **28**, 1360.
Warkentin, P. A., H. J. Haucke, and J. C. Wheatley, 1980, Phys. Rev. Lett. **45**, 918.
Warkentin, P. A., H. J. Haucke, P. Lucas, and J. C. Wheatley, 1980, Proc. Natl. Acad. Sci. U.S.A. **77**, 6983.
Welander, P., 1967, J. Fluid Mech. **29**, 17.
Wesfreid, J., Y. Pomeau, M. Dubois, C. Normand, and P. Bergé, 1978, J. Phys. (Paris) Lett. **39**, 725.
White, G. K., 1959, *Experimental Techniques in Low Temperature Physics* (Clarendon, Oxford).
Wilks, J., 1967, *The Properties of Liquid and Solid Helium* (Clarendon, Oxford).
Yorke, J. A., and E. D. Yorke, 1981, in *Hydrodynamic Instabilities and the Transition to Turbulence*, edited by H. L. Swinney and J. P. Gollub (Springer, Berlin), p. 77.
Zaitsev, V. M., and M. I. Shliomis, 1970, Zh. Eksp. Teor. Fiz. **59**, 1583 [Sov. Phys.—JETP **32**, 866 (1971)].

FIG. 11. A convective pattern observed using a Doppler velocimetry flow visualization technique with computer enhancement (Gollub and Heutmaker, 1984).